Microfluidics for Protein Crystallization and

Mapping Phase Diagrams of Aqueous Solutions

A Dissertation

Presented to

The Faculty of the Graduate School of Arts and Sciences
Brandeis University

Physics Department

Seth Fraden, Advisor

In Partial Fulfillment
of the Requirements for the Degree
Doctor of Philosophy

by

Seila Selimovic

February 2010

This dissertation, directed and approved by Seila Selimovic's Committee, has been accepted and approved by the Faculty of Brandeis University in partial fulfillment of the requirements for the degree of:

DOCTOR OF PHILOSOPHY

Adam B. Jaffe, Dean of Arts and Sciences

Dissertation Committee:

Seth Fraden, Physics Department

Robert Meyer, Physics Department

Dagmar Ringe, Biochemistry Department

Acknowledgements

I wish to express my gratitude to my thesis advisor, Professor Seth Fraden, for his ongoing guidance and support in this research. I further thank my collaborators for their assistance with experiments, especially Dr. Dali Liu and Professor George Thurston, as well as Dr. Frédéric Gobeaux, Dr. Yanwei Jia, Dr. Hakim Boukellal, and Dr. Jung-uk Shim. Special thanks go to the Professor Robert Meyer and Professor Dagmar Ringe for the advice they have given me throughout this doctoral research, and to the faculty, staff, and students of the Physics Department, and of course to my family and friends.

ABSTRACT

Microfluidics for Protein Crystallization and

Mapping Phase Diagrams of Aqueous Solutions

A dissertation presented to the Faculty of the
Graduate School of Arts and Sciences of Brandeis University
Waltham, Massachusetts

By Seila Selimovic

Microfluidic devices are often likened to integrated circuits, mostly for their promise to alter conventional laboratory techniques and, consequently, standard approaches to science. The main premise of microfluidics is namely to transform a wet laboratory to a large degree into a micro-sized device, a so-called lab-on-a-chip It allows users to handle small amounts of liquids inside channels that are tens to hundreds micrometers wide or high, and the devices often require little external infrastructure and can be developed into portable chips. The objective of this dissertation is to demonstrate the application of microfluidics for protein crystallization and, more generally, for mapping phase diagrams of aqueous solutions, such as salts, polymers, and protein. The benefits of our microfluidic platform - the PhaseChip - are manifold: Our crystallization trials are faster and more efficient than conventional crystallization methods, because they are confined to hundreds of nanoliter and even picoliter, rather than microliter sized

droplets; we can subject our aqueous solutions to many reversible cycles of supersaturation by controlling both the temperature of the solutions and the concentration of solutes; and we have developed a Reversible Permeation technology and concentration and temperature driven experimental protocols that allow us to control and decouple crystal nucleation from crystal growth. This is especially advantageous when statistical measurements of crystal nucleation rates are of interest. Lastly, we can generate concentration and temperature gradients across the PhaseChip, both in space and in time, which allows us to study many more crystallization conditions than previously possible. These factors enable us to map phase diagrams of aqueous solutions and identify or optimize previously known crystallization conditions that yield defect-free and large protein crystals.

Table of Contents

Chapter 1. Introduction

Microfluidic devices are often likened to integrated circuits, mostly for their promise to alter conventional laboratory techniques and, consequently, standard approaches to science[8]. The main premise of microfluidics is namely to transform a wet laboratory to a large degree into a micro-sized device, a so-called lab-on-a-chip[9,10]. More specifically, microfluidics is a technology that allows users to handle small amounts of liquids inside channels that are tens to hundreds micrometers wide or high. The devices that contain these channels are usually between 1 cm and 3 cm in radius, and hence are small enough to be developed into portable machines.

Benefits of using such small devices to operate the flow of liquids are manifold. This is easily demonstrated on the example of protein crystallization, one of many applications of microfluidics. Here, various reagents are combined in nanoliter or picoliter sized aqueous drops separated by oil. Thus, in large crystallization trials only microliters of liquids are necessary, which is especially fortunate when expensive reagents are used. Also, instead of manual screening, which is tedious and time-consuming, microfluidics enables high throughput screening. The PhaseChip, a device developed in our laboratory is capable of conducting up to 1600 crystallization trials simultaneously (on a chip that stores 4 nl sized drops) or up to 5000 crystallization trials (on a chip that stores 65 pl emulsion drops), since each drop is an independent chemical

system having arbitrary composition and size[3]. This approach to protein crystallization can be used to construct phase diagrams of multicomponent systems containing protein, buffers, precipitants, and other salts.[4-6]

Overall, microfluidic devices are capable of sensing and manipulating small reagent volumes, particularly biological systems such as proteins and cells, on short time scales and with high resolution. They are inexpensive to manufacture and operate and they reduce the need for large laboratory equipment. Beyond analysis tasks like protein crystallization, there are many other applications for microfluidics in fields as diverse as biodefense, molecular biology, and microelectronics: DNA sequencing and separation, polymerase chain reaction (PCR), electrophoresis, and cell counting and sorting[11].

The current objective of our work in microfluidics is protein crystallization. As described above, our crystallization trials are faster and more efficient than conventional crystallization methods. Additionally, we have developed a Reversible Permeation technology that allows us to control and decouple crystal nucleation from crystal growth by controlling the solute concentration in aqueous droplets. Lastly, we can generate a spatial and temporal temperature gradient across the PhaseChip, which, in combination with the concentration control, allows us to study many more crystallization conditions than previously possible. These factors enable us to identify crystallization conditions that yield defect-free protein crystals large enough to be subjected to x-ray crystallography and even neutron scattering. Understanding the structure of a protein by studying its crystals is crucial, for example in pharmaceutics, where drugs can be engineered to target a specific residue of a protein.

In this dissertation, we discuss the physics of protein crystal nucleation and growth as well as the PhaseChip, the microfluidic platform that allows us to decouple these two processes. We give several examples (polymer and protein) to demonstrate the characteristics and the reliability of the PhaseChip in studying phase diagrams and crystallization conditions. Finally, we focus on the use of the PhaseChip for crystal nucleation studies in Lysozyme, both via protein concentration and temperature control.

This paper is structured as follows: In Chapter two the reader will find a brief introduction of fluid dynamics governing the flow inside microchannels, as well as the diffusion of water across a thin PDMS membrane. A chapter detailing the physics of protein crystallization follows. Notes on the fabrication of microfluidic chips are given in Chapter four. Chapter five offers information about the design of different microfluidic elements such as wells. Chapters six through eight contain the papers we have published and are about to submit to scientific journals on the design and application of the PhaseChip. The appendices contain detailed information on the device processing conditions.

Chapter 2. Flow in microfluidic devices

a) Flow inside microchannels

As has been pointed out repeatedly[1,2], the macroscopic world is governed by gravity and inertial forces, but as a physical system is reduced in size - the characteristic dimensions of microfluidic channels are width (typically 100 μm or less) and height (30 μm) - these factors lose significance and others, like surface tension or diffusion, become important. Viscosity also gains influence on small scales, so much that it results in laminar or parallel flow in simple geometries. Some characteristics of laminar flow are high momentum diffusion, low momentum convection, and time-independent pressure. Three numbers that characterize flow are Reynolds (Re), Peclet (Pe), and Capillary (Ca) Number:

$$\mathrm{Re} = \frac{w\mathrm{v}}{\nu}, \quad \mathrm{Pe} = \frac{U_a h}{D}, \quad \mathrm{Ca} = \frac{U\mu}{\gamma} \tag{2.1}$$

where w is the characteristic distance of the system (e.g. the channel width), v is the velocity scale of the fluid, ν the kinematic viscosity of the fluid (the kinematic viscosity is the ratio of dynamic viscosity to the density of the material), U_a is the average velocity, h the characteristic length perpendicular to the flow (e.g. the channel height), and D the diffusion coefficient of the particle in question. Similarly, U is the flow velocity, μ the dynamic viscosity, and γ the surface tension. The Reynolds numbers

measures the ratio of inertial to viscous forces; for laminar flow Re is small (<500). The Peclet number relates the convective to the diffusive flow in a fluid. Both numbers can be affected by changes in the geometry of a system. Finally, the Capillary number gives the ratio between viscous and capillary forces. The larger the surface-to-volume ratio, the more important the surface tension. The Capillary number is independent of the system dimensions, but not of surface tension. Adding surfactant to a mixture of two immiscible liquids (water and oil), for example, lowers the surface tension between the two and so changes the Capillary number.

It is evident that on micro-scales diffusion of particles in a solution cannot be ignored. The random-walk approach to diffusion yields a diffusion time t and a diffusion constant D

$$t = \frac{d^2}{2D}, \quad D = vl \tag{2.2}$$

where d is the distance traveled, l is the mean free path, and v is the particle speed. Since the diffusion time depends on the square of the traveled distance, it is much shorter in small geometries.

Some diffusion constants are listed in Table 2.1.

Table 2.1. Diffusion constants of relevance in microfluidic systems.[3]

Water in PDMS	**Oil (FC-43) in PDMS**	**Protein in water**	**Salt in water**
$4 \cdot 10^2 \frac{\mu m^2}{s}$	$2 \frac{\mu m^2}{s}$	$10 \frac{\mu m^2}{s}$	$10^3 \frac{\mu m^2}{s}$

Diffusion in microfluidic channels can be exploited in the mixing of liquids. Assume two co-flowing miscible liquids inside a long channel. In laminar flow and at low flow rates, there is an interface between the liquids, across which particles can diffuse, leading to mixing of the reagents (At high flow rates the two liquids are in contact at the interface for a short amount of time, rendering the interface stable and inhibiting the mixing process.). In another example, a toroidal channel is filled with two or more miscible liquids. As the liquids flow around in a circle, they each produce a parabolic flow profile, which acts as a diffusion interface. In the first case, diffusion occurs along the direction of flow; in the second case, it is perpendicular to the flow.

Regulation of solute concentration is another area that relies heavily on diffusion of particles. Two aqueous drops of different salt concentration are stored inside a microfluidic channel, separated by a plug of oil which acts as a de-facto membrane. There is no flow inside the channel. In this crystallization method, drops "communicate" with each other by vapor diffusion of water through the oil. In the effort to equilibrate the chemical potential in both drops, water diffuses from the solution with a lower salt concentration to the one with the higher salt concentration.

b) Flow between microchannels

Being able to conduct protein crystallization in microfluidic devices often requires creating droplets of protein and salts and storing them in a well with indirect access to a reservoir fluid, much like it is done in conventional vapor diffusion methods. These wells are completely surrounded by poly(dimethylsiloxane), the material of choice for microfluidic devices, which is permeable to water, but not to protein or salts. Also, the

size of the drops is chosen so that they either assume a disk-like shape when anchored inside the wells (for 4nl or 20nl drops in our experiments) or spherical shape, in the case of emulsion droplets (on the order of picoliters). Because of that, we can assume one-dimensional planar diffusion of water from the drop through the PDMS membrane into the reservoir and into the bulk of the device.

The flux of water in either direction is

$$J_i = -P\nabla C_i, \quad P = kD \tag{2.3}$$

where P is the permeation coefficient of water, k is the solubility and D the diffusion constant of water in PDMS ($k = 7.1 \cdot 10^{-4}$, $D = 8.5 \cdot 10^{-10} \frac{m^2}{s}$ [12,13]). As presented by Shim[3] , the gradient in water concentration inside the PDMS device is:

$$\nabla C_{res} = \frac{\Delta c}{m} = \frac{c_{drop} - c_{res}}{m}, \quad \nabla C_{out} = \frac{\Delta c}{M} = \frac{c_{drop} - c_{out}}{M} \tag{2.4}$$

where m and M are the of the membrane and of bulk PDMS, respectively, and c_{drop}, c_{res}, c_{out} are the molar concentrations of water in the drop, the reservoir, and outside the device (usually 0 M).

These equations can also be expressed in terms of the concentration of solutes *x*, since $c = W - x$, and W is the concentration of pure water (55 M):

$$-\nabla C_{res} = \frac{\Delta x}{m} = \frac{x_{drop} - x_{res}}{m}, \quad -\nabla C_{out} = \frac{\Delta x}{M} = \frac{x_{drop} - x_{out}}{M} \tag{2.5}$$

We assume that as water diffuses in and out of the aqueous drop, the volume of the drop changes. Since the drop is constrained by the height of the well, we write

$$\frac{dV(t)}{dt} = h\frac{dA(t)}{dt} = \frac{JA(t)}{W} \tag{2.6}$$

Plugging equation (2.5) into (2.6) reveals that solute concentration and drop area are inversely proportional:

$$\alpha = \frac{A_\infty}{A_0} = \frac{x_0}{x_\infty}, \quad \frac{A(t)}{A_0} = \alpha + (1-\alpha)e^{\frac{-t}{\tau}}, \quad x_\infty = \frac{Mx_{res} + mx_{out}}{M+m} \tag{2.7}$$

The dimensionless ratio of drop area at a time *t* and the initial drop area is measured in experiments, and we can use it to extract information about the solute concentration.

In a typical experiment, we lose about 0.3 M of water from a droplet to the outside of the PDMS device. This means that the concentration of the reservoir solution should have a solute concentration 0.3M smaller than the solute concentration inside the droplet. For example, to maintain a 0.5 M salt droplet constant in concentration, the reservoir solution should contain 0.2 M salt. Consequently, to maintain a 0.3 M salt droplet constant in concentration, the reservoir solution should contain pure water.

Chapter 3. Protein crystallization

At the core of our approach to protein crystallization[4-8] using microfluidics is the physics view of crystal nucleation and reversible dialysis. A protein-salt solution can be dialysed against higher-salt reservoir fluid, leading to growth of many small crystals in the protein drop. The path of the dialysis can be reversed, by using a lower-salt solution as the reservoir fluid. Then, most of those crystals are dissolved, leaving only a few large seeds to grow. In this chapter we introduce the mechanisms of both nucleation and crystal growth. Then, in Chapters VI - VIII we will learn how these concepts are translated into experiments.

For crystal nuclei to form, the free energy of the particles has to be increased, as evident in the graph below (Figure 3.1). This is due to the interface energy γ between the crystal and the surrounding liquid. Let us assume, for simplicity, that the crystal nuclei are spherical. Then the free energy becomes

$$\Delta G = \left(4\pi r^2\right)\gamma - \left(\frac{4}{3}\pi r^3\right)\Delta\mu . \qquad (3.1)$$

where $\Delta\mu$ is the chemical potential difference between the crystal and the liquid phase of the protein, and r is the radius of the spherical crystal. As the crystal forms, the chemical potential of the protein in the crystal becomes larger than the chemical potential in the liquid. This difference increases with the growth of the crystal. Once a nucleus has

formed and the crystal grows, the nucleation barrier becomes smaller. The critical nucleus size is inversely proportional to the change in chemical potential:

$$r^* = \frac{2\gamma}{\rho\Delta\mu} \tag{3.2}$$

leading to $$\Delta G^* = kT\left(\frac{16\pi}{3kT}\cdot\frac{\gamma^3}{\rho^2\Delta\mu^2}\right) \tag{3.3}$$

The crystal nucleation rate is $$\Gamma \sim e^{\frac{-\Delta G^*}{kT}} \tag{3.3}$$

A supersaturated protein solution has a large nucleation rate, allowing crystals to grow fast.

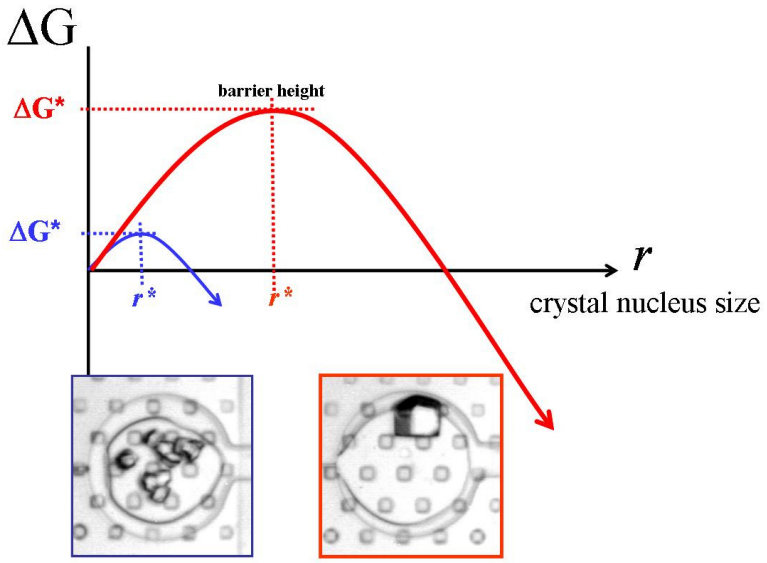

Figure 3.1. Crystal nucleation and growth. ΔG is the free energy, r* is the critical nucleus size, and ΔG* is the nucleation barrier. The micrograph on the left shows precipitation in the protein drop as a consequence of supersaturation. The micrograph on the right shows few large crystals in the drop as a result of increased nucleation barrier.

This nucleation process is shown in Figure 3.2. Assume a stable protein and salt solution, shown in the graph at point a (the red dots stand for different initial

concentrations). At low concentrations (and low supersaturations) the nucleation rate is extremely slow, as is the subsequent crystal growth. Dialysing the solution against a high-salt concentration reservoir solution increases the concentrations of both precipitant and protein. The solution has now moved to the metastable co-existence phase (point b on the tie-line). If the nucleation barrier can be reached, then many crystal nuclei will form, leading the solution to point b' at the co-existence – crystal phase boundary. At this point, crystal growth is rapid, often leading to defects.

Because we prefer single large, defect-free crystals in a drop, we decouple crystal growth from the nucleation mechanism. By changing the reservoir fluid to a low-salt solution we lower the supersaturation level in the protein-salt solution. Water permeates back into the protein drop, decreasing the concentrations of protein and precipitant. As a consequence, most crystals are dissolved ($\Delta\mu$ decreases), and only those of a critical size remain, since both r* and ΔG^* increase. The growth of the remaining crystal is slowed down, reducing the probability of defects. This is represented in the graph with the path from b' to c'.

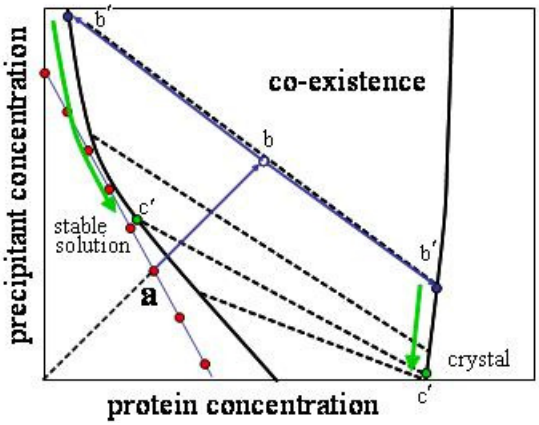

Figure 3.2. Decoupling nucleation and crystal growth. In this phase graph of a protein solution, thick black lines denote phase boundaries. The dashed lines are tie-lines. The initial solution is denoted by red dots. Raising supersaturation will lead to nucleation and

growth of many small crystals. This is represented by a line going from point a (stable solution) to a co-existence point b and, if crystal nuclei are formed, ending with crystals at b'. Lowering supersaturation will dissolve small crystals and grow large crystals. This corresponds to a path from b' to c'.

Chapter 4. Fabrication of microfluidic devices

The fabrication of a microfluidic chip consists of three main stages: design, wafer patterning, and mold making. All stages, including surface treatment of the device and testing, can be completed within one week. Familiarity with the fabrication process and the difficulties that might arise during that process helps us design better devices. Each stage can be easily modified to create devices with two or more layers of channels and different channel heights.

a) Photolithography

We describe here the lithography process for a generic two-layer device (Figure 4.1)[3,14,15]. (Fabrication details can be found in Appendix I.) A silicone wafer is used as a master substrate, on which channel structures are to be imprinted. Negative photoresist such as the epoxy-based SU8 resist (Microchem) is dispensed on the wafer and spun at the desired rate. During spin-coating the resist is first distributed on the whole wafer surface; next, the rate is increased to achieve the desired final height of the photoresist, which for our devices varies between 30 μm and 80 μm. During the following soft bake, solvents in the resist evaporate and the resist starts to harden. When exposed to UV-light (300-400 nm) through a transparency mask, the resist cross-links: a strong acid forms and enhances the hardening process during the post exposure bake. This step ensures that all

solvents evaporate and that the exposed photoresist becomes insoluble to the developer. Finally, the resist that is not cross-linked is dissolved using a commercial developer (1-Methoxy-2-Propanol Acetate, $C_6H_{12}O_3$).

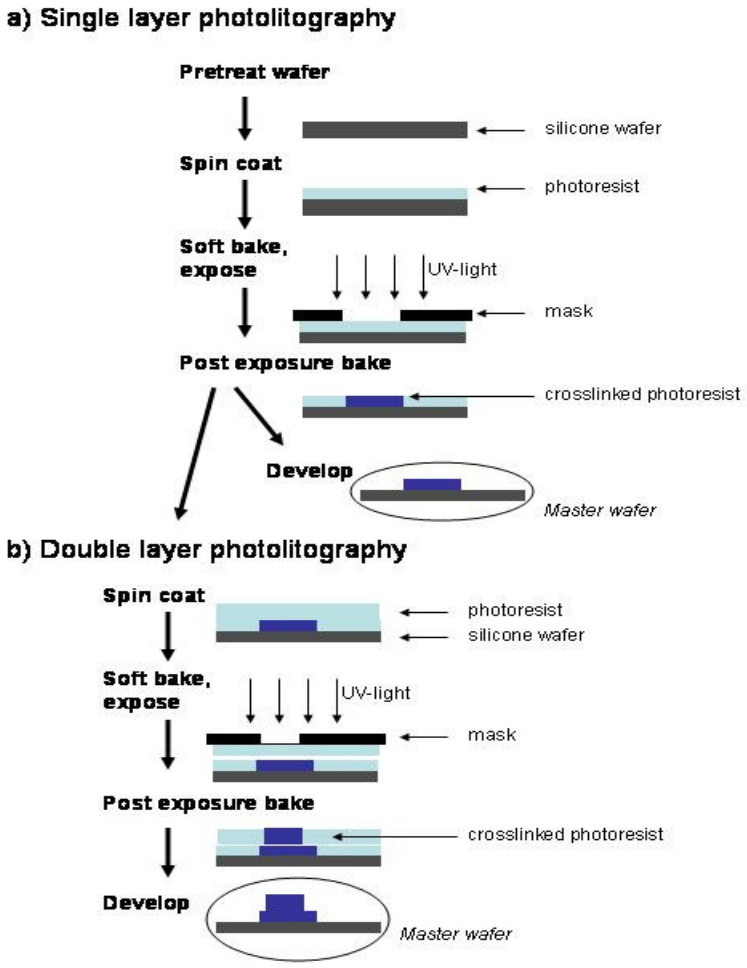

Figure 4.1. Schematic of the photolithography process. A Silicone wafer is cleaned, spin coated with photoresist, soft baked, exposed with UV light and baked again. If channels of uniform height are desired, these steps are followed with developing of the resist (a). If channels of different heights are needed, then another layer of photoresist is applied to the wafer (b), before the resist is developed.

Channels with a rounded cross-section (Figure 4.2) can be achieved using positive photoresist, which is a thermoplastic polymer (AZ 4000 series). This is useful when developing microfluidic elements like valves and pumps (see next chapter). We first vapor deposit Hexadimethylsilanaze ($C_6H_{19}NSi_2$), an adhesion promoter, on the wafer. Then the resist is spun on the wafer, soft baked, and exposed as described above. Exposure to UV light, however, does not harden the material, but makes it soluble to the developer (AZ 400K). After the developing process only the unexposed resist remains on the wafer. In the final step, the wafer is heated above the glass transition temperature of the photoresist. The resist melts and spontaneously forms rounded shapes, which can result in a dramatic change in channel dimensions. During an additional hard bake the resist hardens further and becomes insoluble to solvents like Methanol or Isopropanol.

b) Printing in PDMS – Soft-lithography

The last stage in the device fabrication is printing in PDMS (Figure 4.3). [15-17] Poly(dimethylsiloxane) – PDMS – is a two-part elastomer, consisting of a base and a curing agent (Sylgard 186). Both materials are liquid; they harden or cure only when mixed. The manufacturer (Dow Corning) recommends mixing the two parts in the ratio 10:1, although different ratios may be desired for the device fabrication - we prefer the 10:1 ratio, because it gives the most robust, yet flexible PDMS devices. PDMS is optically transparent down to 230 nm, so it can be used with many microscopy techniques; it is simple to handle in the laboratory, it is flexible and durable, resists high pressures, and is inert to many chemicals[2]. Further, it is permeable to gases and a good substrate for biological systems. Also, many polymer devices can be made from just one

set of master wafers. These factors and the low cost of manufacturing make PDMS a favorable material for the fabrication of microfluidic devices, although glass or plastics can also be used.

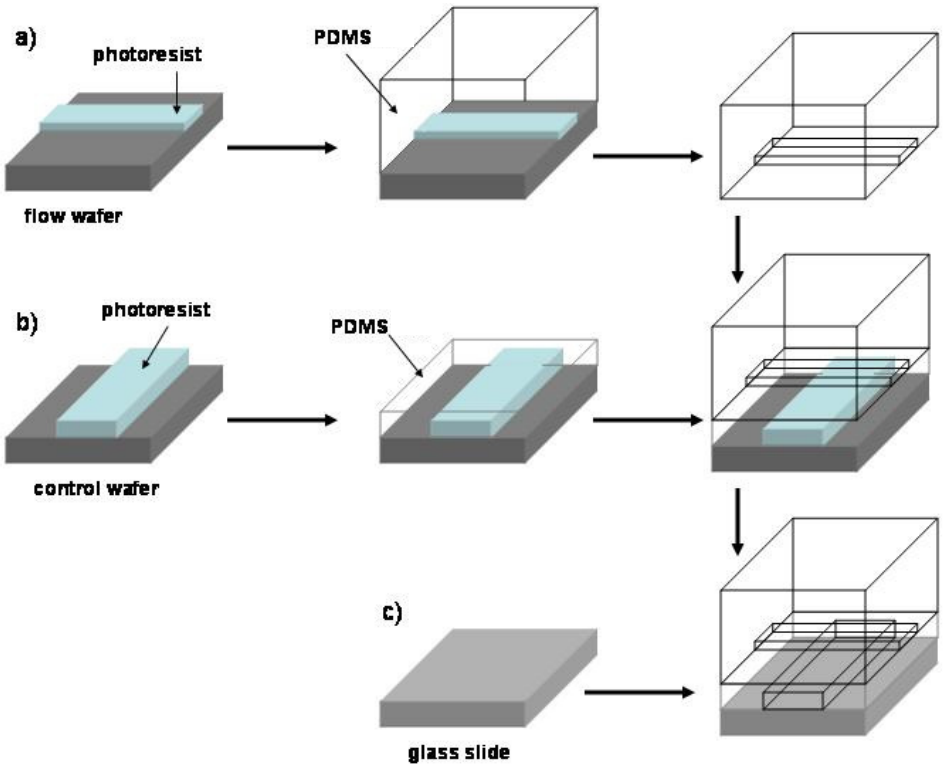

Figure 4.3. Schematic of the mold fabrication process. a) PDMS is poured onto the flow wafer, partially cured, and peeled off, so it can be aligned and bonded to the PDMS layer spun onto the control wafer (b). After curing, both layers are peeled off and plasma bonded to glass (c).

To form a two-layer device we first pour PDMS (base : curing agent = 10:1) on the flow wafer, i.e. the wafer with the flow channel profile. The polymer is then baked to fully cure (Figure 4.4). We cut and peel the now solid slab of PDMS off the wafer; it has the flow channel pattern imprinted in it.

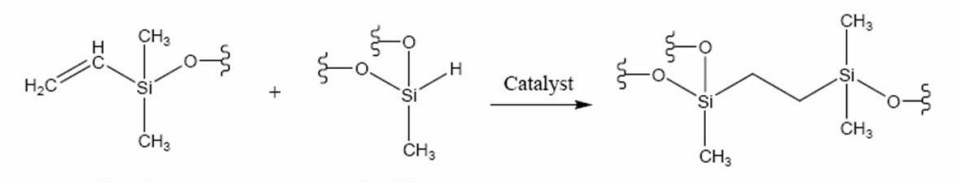

Base + Curing agent -> (via catalyst) solid PDMS

Figure 4.4. Crosslinking of PDMS, catalyzed by heat. Part A is the base, part B is the curing agent. [17]

Next, we vapor deposit Chlorotrimethylsilane ($(CH_3)_3SiCl$) on the control wafer (the wafer with the control channel profile) to prevent irreversible bonding of PDMS to the silicone wafer, and spin coat the wafer with PDMS in the same ratio as for the thick slab (base : curing agent = 10:1). The thickness of this layer is generally 30 μm. After this PDMS layer has fully cured, we expose both layers to oxygen plasma (60 Watt for 8 seconds) and then align them, such that the two patterns are imprinted in each polymer layer overlap in the right places and are separated by a thin layer of spin-coated PDMS, the membrane (~ 30 μm). Heating the two layers of PDMS together increases the strength of the plasma bond between them.

We note that when oxygen plasma is used to bond the layers, that bond is irreversible, i.e. any alignment errors cannot be rectified. (Our design accounts for this and has a built-in error tolerance for up to 300 um in any direction. If the alignment of the two layers must be accurate to within 10 um, then a different bonding mechanism is suggested. In this method, we would use a 5:1 PDMS mixture for the flow or storage layer and a 20:1 PDMS mixture for the membrane or control layer. The two layers should

be only partially cured prior to bonding, such that the excess of base and curing agent can diffuse from one PDMS layer into the other, thereby creating a stronger chemical bond. The benefit of this procedure is that any alignment errors can be rectified by peeling the thick PDMS layer off of the membrane and realigning it. This can be done multiple times, but is not possible with the plasma bonding. A disadvantage of the 20:1 - 5:1 method is, however, that the chemical bond between the two layers is weak compared to plasma bonding, resulting in air bubbles forming between them and subsequent tearing of the membrane.

After bonding both layers can be removed from the wafer together. We drill holes through the device that will act as inlet and outlet ports for both flow and control layer. Later, we connect Tygon tubing to these ports to deliver reagents and air and to remove liquid waste. Because PDMS is a flexible material, we give it rigidity by bonding it to a glass slide using oxygen plasma. Alternatively, we can bond the assembled device to a reflective silicon wafer, also using oxygen plasma. This bond is strong enough to withstand pressures of up to 60 psi, which is beyond the applied pressure routinely used in our laboratory (~5 psi). At 60 psi, tubing connected to the PMDS device for fluid delivery is pushed out of the device, but the bond between the two layers remains intact.

The two methyl groups in dimethylsiloxane monomers render the elastomer largely hydrophobic[2]. The free electron pair of the oxygen atom in the molecule backbone, however, can undergo hydrogen bonding and so cause water to wet the surface of PDMS. Depending on the demands of the experiment, this surface can be chemically modified. To make the surface completely hydrophilic, the device should be exposed to oxygen plasma, which creates surface silanol groups. Conversely, to achieve a fully

hydrophobic PDMS surface, we coat the device channels with a fluorocarbon polymer (CYTOP, Bellex International). CYTOP – 809M is a perfluoro-polymer, consisting of 9% w/w poly(1m1m2m4m4m5m5m6m7m7m-decafluoro-3-oxa-1,6-heptadiene) in perfluorotributylamine. The molecular weight of the coating agent is 60000-70000. The glass transition temperature of this product is 180 C. CYTOP is highly transparent up to a thickness of 200 μm, so it does not alter the optical characteristics of our devices. Treating the device with CYTOP prevents aqueous drops from wetting the channel surface and coalescing.[3] This is especially important, as we need to reliably control the drop size and content during the experiment.

As the last step, Tygon tubing is inserted into the input and output ports of the PDMS devices. It can either be connected to automatic syringes that fill in the reagents or to external pressure valves.

c) Design principles

Familiarity with the fabrication process of microfluidic devices and its difficulties greatly enhances the understanding of the design. Microfluidic chips are routinely developed using computer assisted design (CAD) programs, such as AutoCAD (Autodesk Inc.). There are several rules that should be considered when creating a new design: The smallest dimension of any feature should be 15 μm. This and other values are limiting values in our laboratory. If chrome masks or other photoresists are used, then the minimum feature size can be 1 um or smaller.Design elements smaller than this can be easily damaged during the fabrication process. The spacing between two channels should be on the order of 50 μm or larger. This is to prevent links between two channels that can

occur during further processing, e.g. by a lint particle lying across a channel. Device elements such as valves and pumps (which were used in an early version of our protein crystallization device) are manufactured using positive photoresist, which allows for rounded channels. All other features are fabricated using negative photoresist, which is less sensitive and yields channels with a rectagonal cross-section.

To create channels of different heights, two or more printing masks should be used. Alignment marks that are incorporated in the design greatly enhance the alignment precision. Currently, the error in mask alignment that is accounted for in the design is 10 μm, even though processing errors are smaller. The error in the alignment of PDMS layers is larger, 20 – 100 μm depending on the complexity of the design (the PhaseChip allows for alignment errors up to 300 um). In devices with two or more layers of PDMS, if the valve effect is desired, the flow and the control channel should cross each other with an overlap of at least 100 μm to account for any misalignment of the two layers. Is the valve effect not desired, the width of the control channel has to be much smaller across the flow channel. Typical dimensions for this case are 100 μm for the flow channel width and 15 μm for the control channel width. Other possible choices are listed in the following chapter. Additionally, for multilayer devices the dimensions of all channels in the upper (thick) layer of PDMS should be increased by 1.55% to account for the shrinkage of PDMS.

Chapter 5. Engineering microfluidic devices

In the development of the PhaseChip there were several modifications of the drop formation and storage methods and the drop formulation mechanism. In this chapter we outline some important microfluidic elements we have used in this development and relate their advantages and disadvantages compared with the final product.

a) Control lines: Valves and pumps

In our efforts to expedite the process of screening for optimal protein crystallization conditions, we not only automate the actual screening process, but also the mixing of salt and buffer solutions or the formulation. Such on-chip mixing is enabled with the microfluidic Formulator, a device originally developed by Stephen Quake for screening of crystallization conditions.[8] Our version of this device was used to mix arbitrary volumes of up to sixteen different reagents, such as salt and buffer solutions at various pH values.

At the heart of the formulator is the peristaltic valve[18,19], also developed by Quake. A valve consists of a flow channel embedded in the flow layer of the PDMS device, and a dead-end control channel, which is placed in the control layer. Thus, the two channels are separated by a thin membrane (~30 μm) and are placed so that they cross each other. When the control channel is filled with water and pressurized, the

membrane deflects to increase the volume in the control line and close off the flow in the flow channel: the valve is closed. This is only possible when the flow channel has a rounded profile, which can be achieved with positive photoresist, as explained in the previous chapter. When no pressure is applied to the control channel, flow in the flow channel is uninhibited and the valve is said to be open. It is important to note that valves can only be reliably used with pressure-driven flow. Experiments have shown that lower pressures are necessary to close a valve when the flow channel crosses above the control channel and thus the membrane is deflected upwards (push-up valve) then in the opposite case (push-down valve). In addition, the activation pressure grows linearly with the membrane thickness [cf. [3]]. Typical flow and control channel dimensions for push-up valves used in our devices (membrane thickness ~ 15 μm) can be found in Table 5.1.

Table 5.1. Typical valve dimensions and valve activation pressures. The channel dimensions are in μm and the pressures are in psi. The minimum pressures needed to control a valve can be lower than the listed values.

Flow channel width	100	125	150	200
Flow channel height	17	25	30	30
Control channel width	125	150	200	250
Control channel height	30	30	40	40
Closing pressure	12	15	20	20

A further device element that relies on valves is the displacement pump. A pump consists of three or more valves spaced closely on the same flow channel. The spacing

between two valves corresponds to the width of a valve. The valves are opened and closed in a specific sequence[20]. An example is shown below (Figure 5.1).

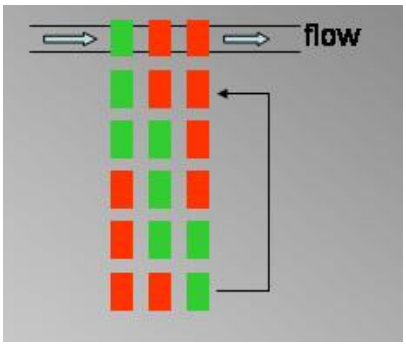

Figure 5.1. A pumping sequence. Blue arrows denote the direction of the flow in the channel. Green bars denote an open valve, red ones a closed valve. The sequence consists of five steps and can be repeated to propel more fluid.

When a valve is closed, the deflected membrane displaces fluid inside the flow channel and prohibits flow. The amount of fluid displaced and propelled during each pumping sequence depends on several factors. First, the higher the flow pressure (and thus the faster the flow rate), the more fluid is propelled when a valve is open. Second, a high pumping frequency (~ 20 Hz) helps propel less liquid per iteration than a low frequency (~ 1 Hz): If the PDMS membrane is driven too fast, it cannot deflect quickly enough in response to the pressure change. As a consequence, the valve is never fully open, thus restricting the flow in the channel. Third, the more often the pumping sequence is repeated, the more fluid is propelled. An obvious, but important benefit of the displacement pump is that it allows the experimenter full control over the flow in the

channel, contrary to volume-driven flow. While a single valve merely stops and resumes the flow, a pump can push exactly metered volumes of fluid inside the flow channel.

This can be utilized to create aqueous drops in oil, or a Drop on Demand. Conventionally, drops in microfluidic channels are formed using flow focusing or a T-junction, both of which are volume-driven methods. There, two co-flowing streams of oil shear off droplets from a continuous stream of water[21,22]. The two variables that control the drop formation are the flow rates of oil and water. The drop production is continuous, and any changes in drop size or drop spacing are gradual. The Drop on Demand method relies instead on pumps to create drops by inhibiting and resuming the flow in channels containing oil and an aqueous solution. First, the pump controlling the flow of oil (oil pump) is turned on, propelling a desired amount of oil into the main flow channel. Next, this pump is replaced by the water pump, which now fills the main channel with the aqueous suspension. This water drop is pushed forward by the next plug of oil, before the water pump is turned on again, and so on (Figure 5.2).

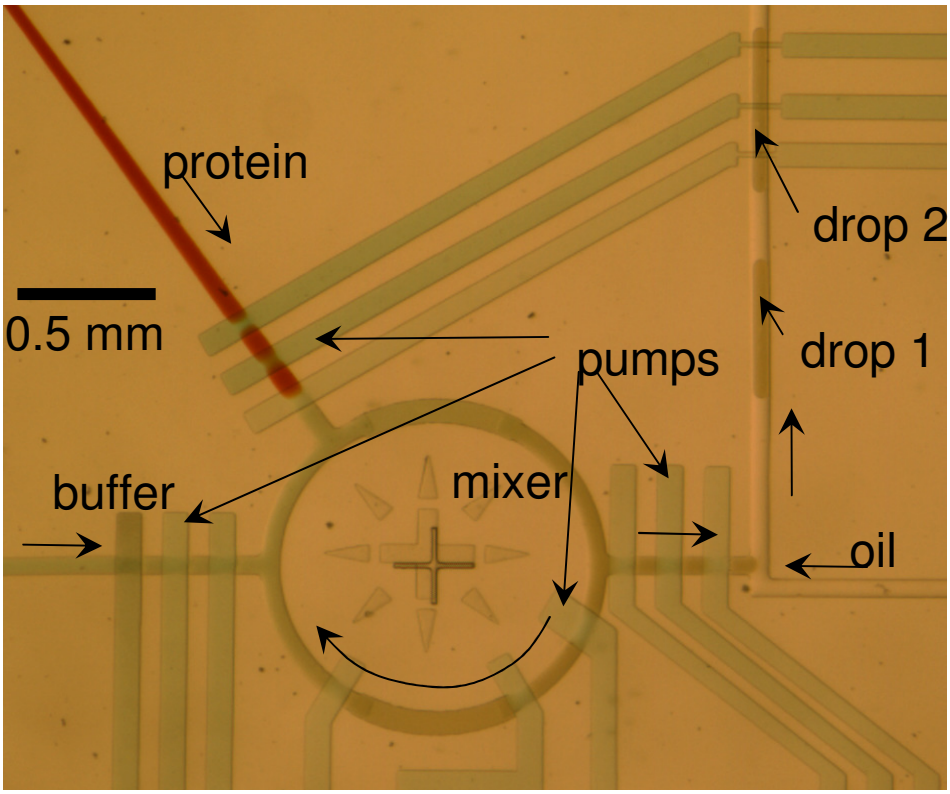

Figure 5.2. Micrograph of a Drop on Demand device. The dead-end channels are the control lines. Different buffers are pumped from the left (green) into the mixer. Protein (red) is also pumped into the mixer and combined with the buffers. The solution is then pumped into the main channel on the right, alternating with oil (white). As a result, long drops of aqueous solution (green) are formed in oil.

This method allows for more control over the drops than the flow-focusing method, because the experimenter works with small flow rates and can thus easily adjust the size of the drops and the spacing between them simply by changing the number of pumping iterations. The size of drops, for example, is controlled by the number of iterations of the water pump, and the drop spacing by the oil pump. Beyond that, drops do

not have to be made continuously, but on demand. The Drop on Demand method is particularly useful in concert with a drop formulation and mixing element. Selecting and mixing the reagents for one drop in such a formulator can last up to 30 seconds. It is only after this period that enough fluid is present in the flow channel to create a drop on demand. When this fluid is released into the main flow channel, it takes time to replenish the water line. This, however, does not affect the spacing between two drops, because the oil pump is independent of the formulator.

b) Drop storage

We have shown how aqueous drops in oil are created and how their contents are formulated. Just like in conventional protein crystallization trials, these drops need to be stored such that they are in close proximity to a reservoir fluid. This can be done in different ways: The approach taken by Ismagilov[6,7]. is to use the flow channel as storage space, where drops remain stationary, separated by plugs of oil. Quake also uses flow channels for storing drops. He employs peristaltic valves to cut off a flow line at several places, using the space between the valves as storage chamber[9].

Our early PhaseChip operates differently, relying on new structures as wells. Drops are stored on the PhaseChip in four different regions, each containing 45 storage chambers[3,23]. These chambers or wells are tall cavities placed on either side of the main flow channel, adjacent to, but in contact with it. We strive for circular wells that are at least 25% taller than the flow channel, although cubic and rectangular wells can also be used (Figure 5.5). While in the flow channel, the drops are compressed, and their shape can best be described as a flattened rectangle with two convex ends. Once a moving drop

encounters a vacancy (empty well), it occupies that well and takes on a spherical shape. Because the well is taller than the flow channel, the center of mass of the drop shifts upwards, resulting in a gravitation energy gain. The surface tension of the spherical drop, however, is smaller than that of an elongated drop. Overall, the drop reduces its total energy by assuming a spherical shape, which is why it can be trapped and stored inside a well.

If the well is tall enough, then the drop is permanently anchored inside it and it cannot be displaced by the next drop. If the well is shallow, however, the stored drop will be displaced as the next drop fills this well. We have mentioned previously that aqueous drops should be prevented from coalescing, and their contents should be kept separate. This becomes difficult when drops pass each other in the storage region on their way to the next empty well. Drops can be stabilized against coalescence by adding surfactant to the oil. We use fluorinated oil as drop carrier (FC-43) - Perfluorotributylamine, 3M; molecular weight: 670; molecular formula: $C_{12}F_{27}N$; kinematic viscosity: 2.5 cSt - , because it has low permeation through PDMS and low viscosity, so it can easily be controlled with valves[3]. To the oil we add fluorocarbon polymer (15% v/v) as surfactant. This combination ensures that a drop passing by a filled chamber does not coalesce with its neighbor.

c) Store, then create method (parts of this section are reproduced by permission from the Royal Society of Chemistry from: Boukellal, H; Selimovic, S; Jia, Y; Cristobal, C; Fraden S. *Lab Chip*, **2009**, *9*, 331-338.)

A major disadvantage of the drop-on-demand technique is that it relies on valves. Valves can only be fabricated using the 20:1 - 5:1 PDMS bonding technique (described in the previous chapter), because the alignment of the two device layers is very important and sufficient precision cannot be achieved when using oxygen plasma for bonding. Hence, the device fabrication is difficult to control and the yield of functioning devices is low (60-70%). This raises the cost per device and delays the experimental progress. Additionally, there is a start-up period associated with this method, during with precious solutes (e.g. protein) are wasted.

We therefore decided to develop a new drop formation technique that relies on the flow channel geometry rather than on control valves and does not require a start-up period. This new method of creating drops is coupled with drop storage. and is driven by a continuous flow of oil. This method, which we call “create, then store” is passive in the sense that in operation only a steady flow of fluid through the device is required. The droplet, created upstream from its storage location, is guided by a combination of hydrodynamic flow and capillary valves into a storage well. Figure 3 shows a single storage element consisting of a main channel that enters a junction with two channels on the exit. One channel, labeled the “well”, begins as a continuation of the main channel and then narrows by a factor of ten at a restriction. There is a second channel labeled the “bypass” oriented at 90 degrees to the main channel and of half the width that serves as an alternative flow path when the well is occupied. At the junction between the well and the bypass the flow coming from the main channel splits into two parts. For a single phase fluid the splitting of the flow between the two channels depends solely on their respective hydrodynamic resistances. However, when a drop enters a junction between

two channels, a combination of capillary forces and the relative hydrodynamic resistance of the channels determine whether or not a drop will go through one channel or another, or even break into two drops.

The fractions of the total flow from the main channel that enters the bypass and well channels were measured by co-flowing a stream of water with dye next to a clear water stream, as shown in Figure (4).

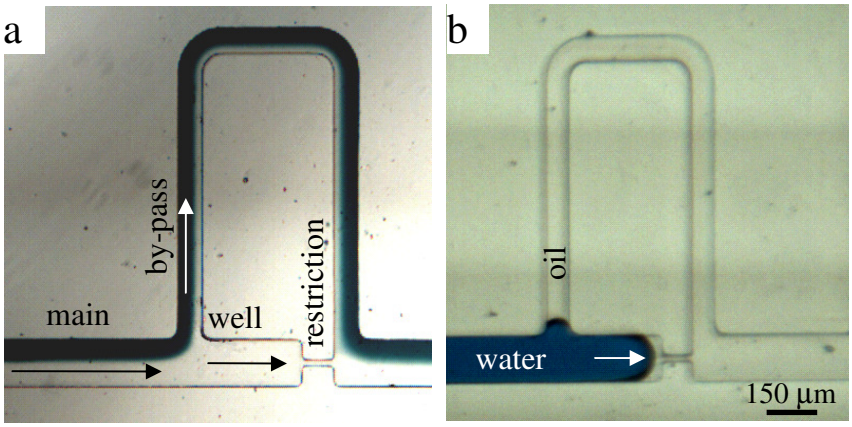

Figure 5.3. Hydrodynamic resistance of channel network. (Reproduced by permission from the Royal Society of Chemistry from Boukellal et al, *Lab Chip* 2009) **(a)** Clear and dyed water are introduced as co-flowing streams in the main channel and bifurcate at the junction of the by-pass and well channels. Dyed water occupies 48% of the main channel and 70% of the by-pass channel implying that 70% of the total flow is carried by the by-pass channel and 30% flows through the well. **(b)** The device is filled with transparent oil and then a plug of colored water is flowed into the device. Although the resistance of the by-pass is much less than the well, none of the water enters the by-pass until the water completely fills the well, demonstrating that the by-pass functions as a capillary valve.

In the case shown in Figure 3 all of the dye flows into the bypass so the following relationship holds: $m_{dye} = b_{dye}$ where m_{dye} and b_{dye} are the dye currents [vol/sec] in the main and bypass channels, respectively. The dye currents are a fraction of the total current in each channel; $m_{dye} = f_m m$ and $b_{dye} = f_b b$ with m and b the total currents in the main and bypass channels, respectively, and f_m and f_b the fraction of dye in the main and bypass channels, respectively. Conservation of flow states that $m = b + w$, with w the total flow in the well. Therefore, the fraction of the total flow that flows down the bypass channel is $b/m = f_m / f_b$. The fraction of dye in each channel was measured using the Plot Profile function of Image J (http://rsbweb.nih.gov/ij/) directly from the photograph in Figure (4) (f_m = 0.48, f_b = 0.70), from which we determine that 70% of the flow goes down the bypass and the remaining 30% of the flow enters the well. The expectation is that the flow would take the path of least resistance, but instead the aqueous plug enters the empty well rather than the by-pass.

This method, which we call "store and create" (Figure 4), allows us to create hundreds of drops on a chip with zero loss. Instead of storing a sequence of pre-formed drops into a series of wells, we flow a long plug of aqueous sample containing no surfactant whose volume is many times that of an individual well into a device completely pre-filled with oil (no surfactant is required). The aqueous plug is then followed by oil. The sequence of steps to create and store drops is illustrated in Figure 4 The priming of the device with oil is not strictly necessary as an air-water interface at the restriction would also function as a capillary valve. But because PDMS is permeable to air, after some short amount of time the air in the restriction would diffuse into the PDMS and vanish. Without an air-water interface the restriction would no longer function as

capillary valve. Therefore we use fluorinated oil as it has a very low solubility in PDMS. The number of wells filled is the ratio of the volume of the aqueous plug to the volume of a single well.

Advantages of this device are that it is simple to manufacture, robust under operation, and drops never come into contact with each other making it unnecessary to stabilize drops against coalescence. Additionally, this device stores all the fluid introduced, including the first amount, with zero waste (we achieve a fill rate of 95%).

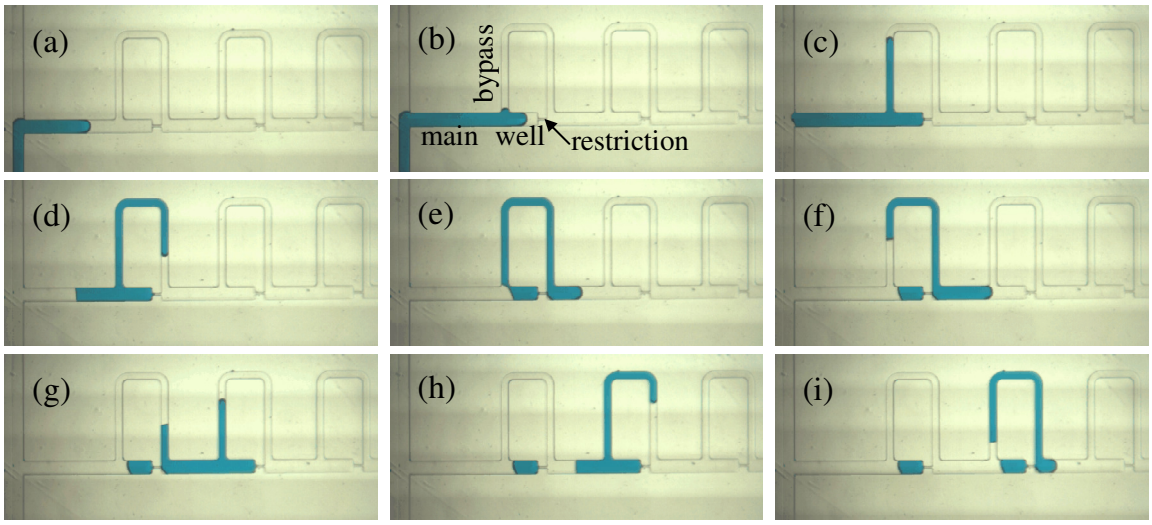

Figure 5.4. Store and create drops. (Reproduced by permission from the Royal Society of Chemistry from Boukellal et al., *Lab Chip* 2009.) **(a)** Initially the entire by-pass storage device (see Fig. 1) is primed with clear oil. Dyed water is flowed into the device. **(b)** Water enters the well, but not the by-pass. **(c,d)** Once the well is filled the by-pass capillary valve opens. **(e, f)** The oil, which is pushing the water, cuts the water stream in two creating a drop in the first storage well. **(g, h)** The water fills the second well and opens the second by-pass capillary valve. **(i)** The oil cuts the water stream in the second well creating a drop in the second storage well.

d) Surface treatment

A major problem in the early protein experiments was the fact that the protein tends to coat PDMS channel walls. This is not very noticeable in the drop fabrication and storage method that relies on nozzles and vales, because the flow rates in that case are high (200 - 300 μl/hr), so we suspect that the protein is never long enough in contact with a patch of PDMS to firmly attach to it. In the "store, then create" method, however, the flow rates are on the order of 50 μl/hr, and we inject a plug of protein solution that is several centimeters long, so there is plenty of time for the protein to attach to the channel walls. This is problematic, because then we do not know how much protein remains in solution, and every drop can have a different concentration of protein. To find the appropriate combination of carrier fluid (oil) and surfactant, as well as PDMS processing for protein experiments, we tested the following variables:

1.) PDMS material: Sylgard 184 vs. RTV

2.) age of PDMS device: we suspect that a fresh device has more hydrophilic sites due to the plasma bond

3.) choice of surfactant: Zonyl FSO-100, Mw=725 ((C2H4O)x(CF2)yC2H5FO); Zonyl FSN-100, Mw=950; Tridecafluoro-1-octanol, Mw=364 (C8H5F13O); a proprietary non-ionic triblock surfactant kindly provided by Raindance Technologies, Inc. (Krytox FSH - b- PEG600 -b- Krytox, and Krytox: F-(CF(CF3)-CF2-O)x-CF2-CF3). These surfactants were mixed with FC43 oil. We chose this oil because it does not swell PDMS, it is fluorinated, which makes it inert and hence desirable for protein studies, and it does not lower the surface tension of the aqueous drops. (If the surface tension of the drops

becomes too small, then the drops tend to break up even when they are stored inside the well and escape through the thin restriction channels.)

We loaded a Lysozyme solution into the PhaseChip (17.5 mg/ml) and observed the change in contact angle between the protein drop inside a well and the surrounding PDMS. When the contact angle is larger than 90° over the course of 6 hours, the choice of PDMS material and surfactant is appropriate. The optimal choice is the following: Sylgard 184, one or more days old, treated with Cytop (see Appendix). The best surfactant choice is Tridecafluoro-1-octanol, dissolved to 12% v/v in FC-43. Using a higher concentration of this surfactant does not offer any improvements in terms of the protein sticking to the PDMS walls. Figure 5.5 offers a few examples of protein sticking to the PDMS and, for contrast, the optimal case.

a)

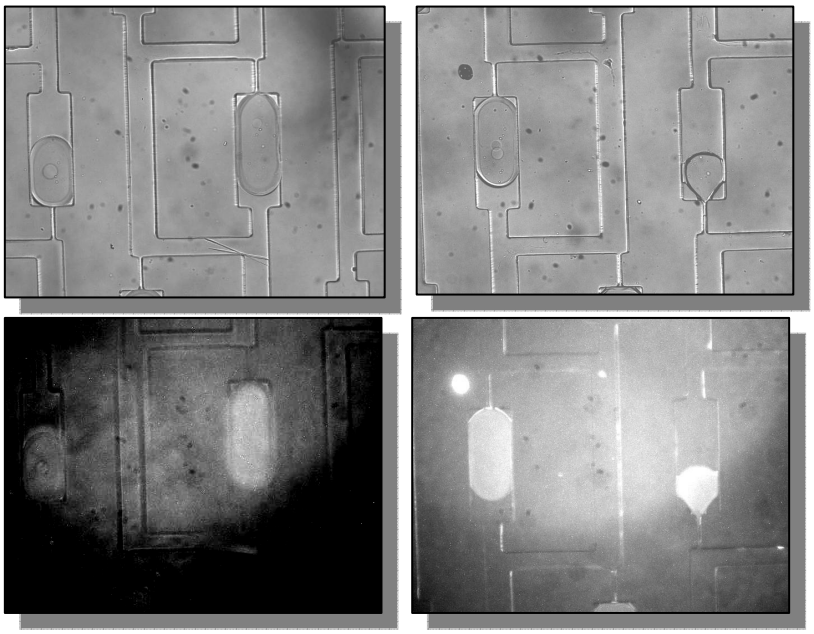

b)

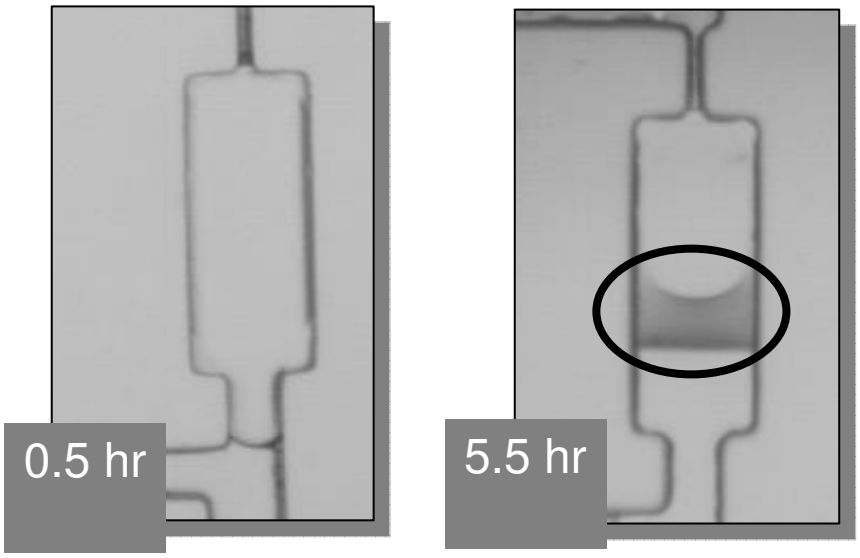

Figure 5.5 Two Lysozyme drops stored in the PhaseChip. Left: immediately after loading. Right: One hour later. The top two photographs are brightfield images, while the bottom photographs are fluorescence images. Note that the fluorescence signal is confined to the drops, indicating that no protein sticks to the PDMS walls along the main channel. (Sylgard 184, Cytop, 1-day old PDMS, FC43 + 12% Tridecafluoro-1-octanol.)
b) A typical protein drop wetting the surface of the PDMS. Left: 0.5 hours after the drop is loaded the drop appears non-wetting. 5.5 hours later, however, a protein film coating the bottom of the storage well has developed (circled), and the contact angle between the aqueous drop and the hydrophobic PDMS surface is 90 °C.

e) Reservoir

The original PhaseChip device had five fully independent reservoir channels. Each channel had a separate input and output. This means that the experimenter had to

prepare five different salt solutions to be used in the reservoir for concentration gradients. This is problematic, because five solutions of different concentrations are not sufficient to explore a wide concentration gradient inside the drops, and because it is easy to make a mistake and prepare the wrong salt concentration in a solution. From the design standpoint, this reservoir was not optimal, because inlets and outlets require a lot of space on a transparency mask that is better used for more important microfluidic elements. We then decided to follow the approach taken in the group of George Whitesides and create a linear gradient reservoir. (This is explained in detail in Chapter VII.) This reservoir has only two inlets for two different salt solutions, next a treelike structure of channels in which the two solutions mix via diffusion, and finally twelve parallel channels, each carrying a different concentration of salt. By choosing a low flow rate (20 μl/hr per solution), we can ensure that the resulting gradient of salt concentrations is linear. Thus, if the injected solutions carry O and 1 M NaCl, then the resulting gradient will contain solutions of 0, 0.1, 0.2, 0.3, etc. up to 1 M NaCl. There is only one exit at the opposite side of the device, for waste collection.

Chapter 6. Measuring the nucleation rate of Lysozyme using microfluidics

Šeila Selimović, Yanwei Jia, Seth Fraden

(Reproduced with permission from *Crystal Growth & Design* **2009**, *9* (4), 1806–1810.

Abstract

We employ the PhaseChip, a (poly)dimethylsiloxane (PDMS) microfluidic device, for statistical studies of protein crystal nucleation. The PhaseChip is designed to decouple nucleation and growth of protein crystals and so improve their yield and quality. Two layers of fluidic channels containing salt reservoirs and nanoliter-sized wells for protein drops in oil are separated by a thin PDMS membrane, which is permeable to water, but not to salt or macromolecules such as protein. We reversibly vary the supersaturation of protein inside the stored droplets by controlling the chemical potential of the reservoir. Lysozyme in the presence of sodium chloride is used as a model system. We determine the crystal nucleation rate as a function of protein supersaturation by counting the number of crystal nuclei per droplet, as demonstrated by Galkin and Vekilov.[24]

Introduction

In this paper, we determine the nucleation rate of a protein crystal as a function of supersaturation at constant temperature using a microfluidic device previously described as the PhaseChip[25]. In brief, the PhaseChip is a two-layer microfluidic device composed entirely of PDMS. The top layer contains hundreds of droplets of protein solution stored in 2.8 nl wells and separated from each other by fluorinated oil. The second layer contains channels through which salt solutions flow. The two layers are separated by a thin membrane of PDMS, which is permeable to water, but not to protein or salt. Thus the second layer acts as a chemical potential reservoir. The difference in chemical potential of water inside the reservoir and inside a drop drives the flow of water across the membrane. Depending on the direction of this gradient, water flows either into the protein drops, thereby swelling them and lowering the solute concentration or out of the drops, therefore shrinking them and raising the solute concentration. Several independent reservoirs are fabricated on the chip, providing both spatial and temporal control over the protein concentration in the drops. Because the contents of the drops are isolated from each other by the fluorinated oil, each drop on the chip acts as an independent, sealed protein crystallization experiment.

One of the key attributes of the PhaseChip is that this design allows many different crystallization conditions to be tested simultaneously, since we can independently change the concentration in different sets of drops. More importantly, the concentrations of the solutes can be reversibly varied by changing the reservoir concentration allowing multiple cycles of supersaturation per sample without having to open the device. Other microfluidic systems that control the solute concentration, e.g. those developed by Ismagilov and Quake[43,44], do not offer such wide range of control. The crystallization system developed by Quake utilizes free interface diffusion, and the

Ismagilov approach uses microbatch droplets, however neither method is reversible. Crystallization methods that are based on temperature quenches, like in the case of Galkin and Vekilov are reversible, but the portions of the phase diagram accessible in a temperature quench are different than in a concentration quench. .

We base our analysis of nucleation rates on the treatment employed by Galkin and Vekilov,[24,26] . In their experiment, a temperature quench is used to change the protein supersaturation. The protein drops there are on the order of μl in volume, which is 100 times larger than in our case. The droplets are first cooled down to a nucleation temperature of 12°C to increase the supersaturation of protein. Next, the temperature is increased to 20°C, which lowers the protein supersaturation and is thus favorable for the growth of few large crystals. A comparison of our results with those of Galkin and Vekilov indicates a qualitative match, but also some notable quantitative differences. The error involved in the measurements presented here is large, but we propose simple ways of reducing it, promising significantly improved performance. Our results suggest that the PhaseChip design can be incrementally modified to develop a crystallization method that is easy to implement, offers convenient control of protein supersaturation, is high throughput, and uses small amounts of protein.

Experiment

Materials

The PhaseChip employed here houses over three hundred protein drops in individual wells. The protein solution is first prepared and filtered off-chip (0.2 μm syringe filter, Corning, product number 431212) and contains 17.5 mg/ml Lysozyme (6x crystallized, Seikagaku), 50 mM NaAc at pH 4.5 and 0.5 M NaCl (Fisher). Then, protein

drops are formed on-chip in a 50 μm nozzle flow-focusing geometry using fluorocarbon oil (Perfluoro compound FC43, Acros) with surfactant (12% w/w 1H,1H,2H,2H-Perfluoro-1-octanol, Fluka).[25,26] The surfactant lowers the surface tension and facilitates the drop formation. It also slows (though it does not prevent) drop coalescence. On-chip valves allow us to direct the flow to a waste line or, once drop formation is stabilized, to one of the four storage regions, each of which contains 62 drops on average. We expect the small number of drops to be a source of significant statistical error. In the experiment described in this paper, all aqueous drops have the same composition. The well volume is 2.8 nl; the initial drop volume is usually smaller, on average 1.4 nl and varies between 900 pl and 2.8 nl. The complete storage region with all 300 wells is 2 cm x 2 cm in size. The protein drops are at all times surrounded by oil and chemically isolated from each other, because solutes do not pass between them. The storage channels are connected to a supply of oil so that as the drops swell and shrink oil flows into the device to compensate for the change in volume.

Underneath and separated from the wells by a water-permeable PDMS membrane (20 μm thickness) are five independent reservoir channels. Each of them is connected to a different bottle of NaCl solution with 0.5 m long Tygon tubing (0.48 mm ID).

Experimental procedure

All 310 stored protein drops have the same initial conditions. During the loading of drops into storage wells all reservoir channels are filled with a 0.5 M NaCl solution, the same concentration of salt inside the drops. This prevents the concentration of solutes in the drops from changing before the experiment begins. After the drops are loaded, a 4M NaCl solution is filled into all reservoirs and kept flowing for a quench time Δt,

which varies for each reservoir. The device is placed on an automated movable microscope stage with a 4x objective lens with a resolution of 10 μm. We periodically record images of the protein drops, which allows us to measure the size of the drops and thus changes in protein and solute concentrations and to record the appearance of crystals. The volume of the drop and shape of the wells are such that the drops take on a disk-like shape inside the storage wells, and the height of the drops is constant at all times. Hence, the change in drop volume only depends on the change in drop area, which we measure using automated image recognition software (NI Vision Assistant). Protein and salt concentrations in the drop at time t are then obtained from the drop area $A(t)$, the initial area A_0, and the known initial concentrations. The solubility values for Lysozyme in NaCl at pH 4.5 are taken from the literature.[29]

During the quench the drops shrink and both the protein and salt concentrations increase, two independent factors which increase the supersaturation. At a particular salt concentration, the supersaturation is calculated as C/C_s, where C is the protein concentration in the drop and C_s the equilibrium protein concentration (solubility) at this specified salt concentration. After this quench time, a 0.6M NaCl solution is introduced into the reservoir channels. The quench times are 4.0, 4.5, 5.0, 5.5, and 6.0 hours for reservoirs R1-R5, respectively. There are on average sixty-two drops exposed to each reservoir condition. As a consequence, each set of drops experiences a different level of supersaturation, depending on the quench time Δt, as shown in Figure 1.

The drops coupled to the first reservoir (R1) develop the lowest protein supersaturation, because they were exposed to a 4M NaCl solution for the least amount of time; conversely, the drops in exchange with R5 are the most supersaturated. Longer quench times result in higher protein supersaturations only when the quench times are

shorter than the time for the drop and reservoir to equilibrate. The equilibration process is

a) nential with a time constant of 30 hours Error! Bookmark not defined. b)

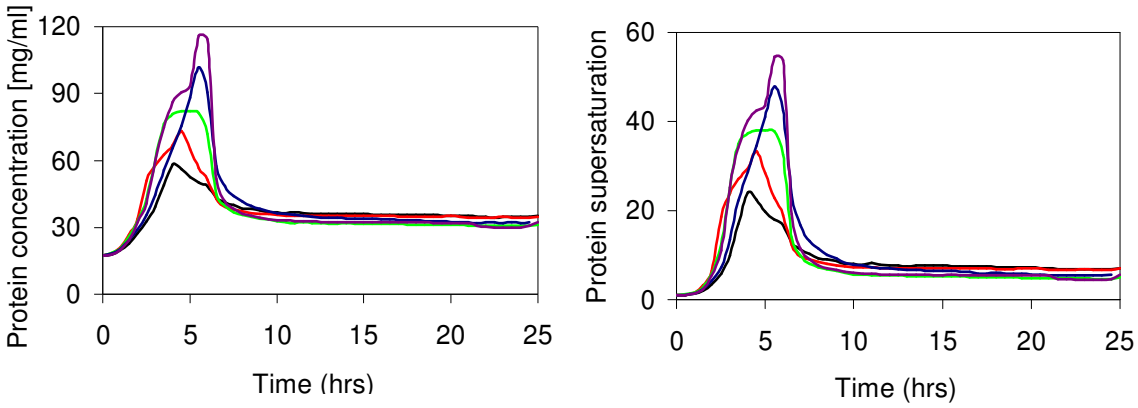

Figure 1. (a) Protein concentration (C) and **(b)** supersaturation (C/C_s) in five sets of droplets with 4M NaCl in the reservoir. Black lines: reservoir 1 (R1) with quench time Δt = 4 h. Red: R2 with Δt = 4.5 h. Green: R3 with Δt = 5 h. Blue: R4 with Δt = 5.5 h. Purple: R5 with Δt = 6 h. (Online in color.)

In the work of Galkin and Vekilov[24], temperature and thus supersaturation changes rapidly. Their experiment was designed such that drops were exposed to a single supersaturation level for different periods of time. In contrast, in our case, the supersaturation was continuously varied.

Results and discussion

Analysis of the drop images indicates that crystals grow during the low supersaturation period following the quench, so we conclude that all crystals have nucleated at the high supersaturation during the quench. This indicates that we have decoupled crystal nucleation from the growth process.

Figure 2 is a photograph of the PhaseChip showing protein drops containing crystals 118 hours after the start of the experiment. The majority of the drops above reservoir R1, corresponding to the lowest supersaturation, have no crystals. Conversely, all drops above reservoir R5 at the highest supersaturation have at least one and often more crystals. This observation is qualitative proof that a) the PhaseChip allows different crystallization conditions to be tested independently and simultaneously, and b) the supersaturation levels of protein inside every drop can be controlled.

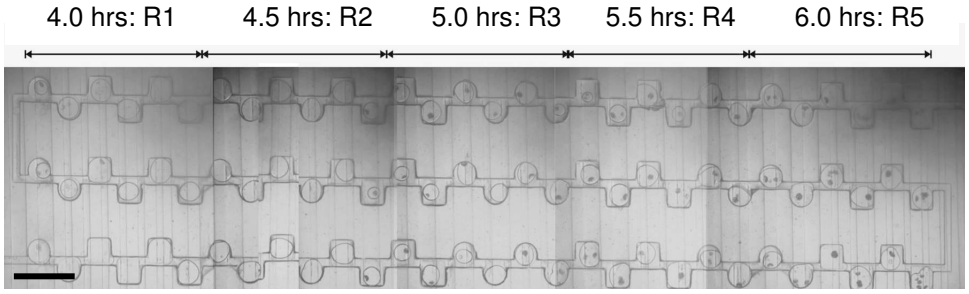

Figure 2. Protein crystals obtained on the PhaseChip for different quench times. On the left side of the device, the quench time is shortest (4 hours) and hence the supersaturation is lowest, so only few crystals nucleate. On the right side, the quench time is longest (6 hours), the supersaturation is largest and there is one or more crystals per drop. The scale bar is 500 μm.

Crystal nucleation is a stochastic phenomenon, so we evaluate our data and calculate the crystal nucleation rate by applying statistical methods. In accordance with the approach developed by Galkin and Vekilov[24] we count the number of drops containing *m* number of nuclei and normalize the distribution. We are interested in how well our data can be described by the Poisson distribution (Figure 3) and compute χ^2 values[28]

$$\chi^2 = \sum_m \frac{\left[N_{trial}P(m) - F(m)\right]^2}{N_{trial}P(m)}. \qquad (6.1)$$

Here, N_{trial} is the number of drops exposed to one particular condition; $F(m)$ are the measured frequencies and $P(m)$ is the Poisson fit. The χ^2 values indicate poor agreement between our data and the Poisson law.[29] One reason is the small number of droplets per reservoir condition, making our system very sensitive to noise. Secondly, there are a few drops with eleven and twelve crystals each, while most drops at those conditions have three to four crystals. We believe that the formation of that many crystals per drop is at least partially due to heterogeneous nucleation, and as such it skews our homogeneous nucleation rate measurements.

We fit this data to the classical nucleation model,[30,31,32,33] in which the nucleation rate J [number of crystals / volume · time] can be expressed as

$$J = ACe^{\left(\frac{-B}{\sigma^2}\right)} \qquad (6.2)$$

$$\text{where } \sigma = \ln\left(\frac{C}{C_s}\right).$$

The parameter B is related to the surface tension γ of the nucleus,

$$B = \left(\frac{16\pi}{3}\right)\frac{\Omega^2\gamma^3}{\left(k_bT\right)^3}, \qquad (6.3)$$

[37]

and A is a measure of the kinetics of nucleation.[34,37] Analytic expressions for this prefactor vary considerably depending on the details of the theory, but in general A is also a function of supersaturation (and precipitant concentration). He and Attard[35] and Moody and Attard[36] have shown that the surface tension decreases with increasing supersaturation. In the range of supersaturations at which most crystals nucleate in our experiment (C/C_s = 24 to 55), however, the surface tension varies little. Hence, we make

the approximation that both quantities A and B are independent of the protein supersaturation. In our experiment, the drop volume V and therefore the concentration C, solubility C_s and nucleation rate J change with time.

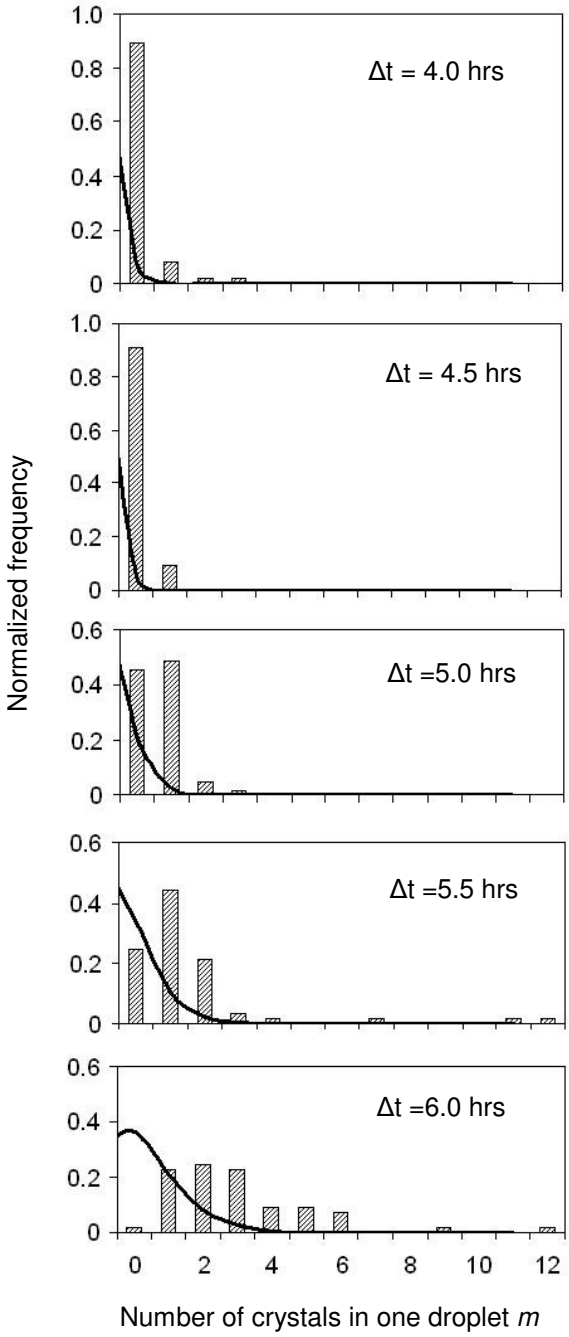

Figure 3. Distribution of *m* Lysozyme crystal nuclei per droplet for different quench times. The shorter the quench time, the lower the protein supersaturation inside the drop and the fewer crystals nucleate.

With these approximations we can calculate the number of crystals per drop as

$$N = \int_0^\infty V(t)\, A\, C(t)\, e^{\frac{-B}{\sigma(t)^2}} dt\,, \tag{6.4}$$

where we treat A and B as constants. We measure the average number of crystals, N_{exp}, per drop at times long after the quench.

We exploit this integral relationship by applying an optimization algorithm, based on Matlab's non-linear least square fit (lstsqnonlin). The algorithm has two parts: 1) It takes as inputs into equation (4) the supersaturation data as a function of time for each of the five quench profiles and 2) it computes the single values of A and B that give the best match between the calculated mean number of crystals per drop N and the measured values N_{exp} for all five data sets simultaneously. Having obtained the best fit values for A and B we plot the extracted nucleation rate $J(t)$ in Figure 4. The nucleation rate is highest for the profile with the longest quench time, since it obtains the largest supersaturation.

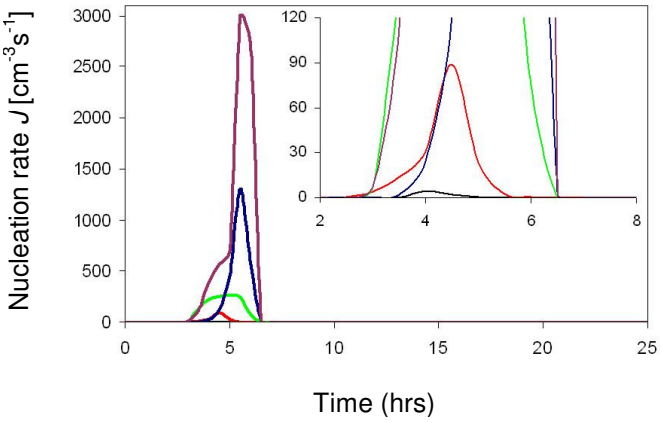

Figure 4. Deduced nucleation rate J of Lysozyme in presence of 0.5M NaCl and 0.05M NaAc at pH 4.5, as a function of time. The inset is a close-up of the main graph. The different curves describe J for different quench profiles. (Online in color.)

The fit gives $A = 6.2 \cdot 10^5$ $mg^{-1}s^{-1}$ and $B = 160$. For comparison, the values of Galkin and Vekilov[24] are 18 $mg^{-1}s^{-1}$ and 65, respectively. The source and meaning of the large discrepancy in our values for A are unclear to us. The exponential term in the expression for J, however, is better understood and more important in characterizing the physical system. Consider equation (3), where Ω is the protein molecular volume ($3 \cdot 10^{-20}$ cm^3) and $k_B T$ is $4.14 \cdot 10^{-21}$ J. We can then determine the surface tension γ of the critical cluster, again assuming that γ is independent of the supersaturation. Our calculation yields $\gamma = 0.91$ mJ/m^2, which is in agreement with literature values for these crystallization conditions[32] (0.8 to 1.1 mJ/m^2), although somewhat larger than the value reported by Galkin and Vekilov (0.64 mJ/m^2). Another way to assess the validity of our numerical results is to plot the experimental values for N_{exp} as a function of quench time Δt and compare them to the values calculated from the optimized A and B constants (Figure 5). Data from five independent measurements of N_{exp} are fitted with two parameters (A, B). The fact that the redundant theoretical and experimental results are in good agreement supports the model's validity.

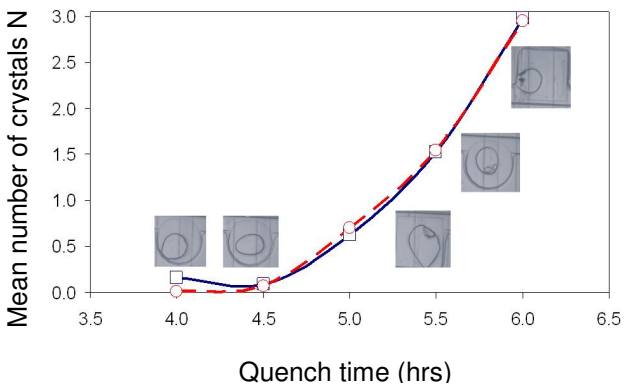

Figure 5. Mean number of crystals N per drop as a function of quench time in hours: Measured values (blue squares) and calculated results (red circles). The lines are a guide for the eye. The images show typical drops from each quench profile. The scale bar is 300 μm. (Online in color.)

Using the fitted values for A and B we can deduce the nucleation rate J at $C_s = 5$ (the regime tested by Galkin and Vekilov). We find it is of the order of 1 crystal nuclei/cm^{3}s or less, which is several orders of magnitude smaller than reported by Galkin and Vekilov at the same supersaturations (Figure 6).

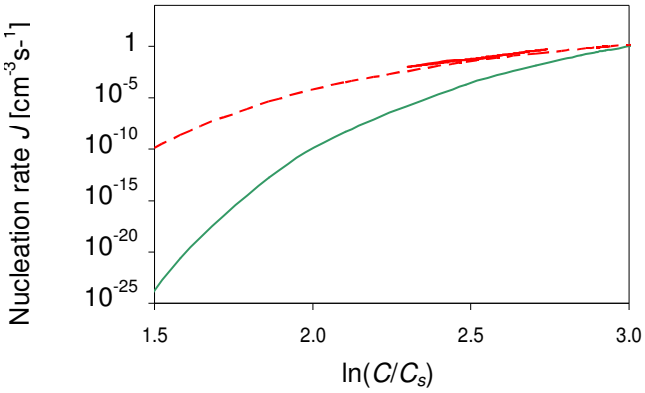

Figure 6. Crystal nucleation rate J as a function of supersaturation. Solid (thin) green curve: nucleation rates calculated using our fitting parameters $A = 6.2 \cdot 10^5$ mg^{-1}s^{-1} and $B = 160$ (extracted from a crystallization experiment with initially 3.5% NaCl), for protein solubility $C_s = 5$ mg/ml and a range of protein concentrations (20 mg/ml to 100 mg/ml). Dashed red curve: nucleation rates calculated using the fitting constants of Galkin and Vekilov ($A = 18$ mg^{-1}s^{-1} and $B = 65$, extracted from a crystallization experiment with 2.5% NaCl). Solid (thick) red curve: experimental data of Galkin and Vekilov at $C_s = 5$. (Online in color.)

We suspect the following to be causes of the discrepancy between our results and those of Galkin and Vekilov.

1.) We cannot exclude the possibility of heterogeneous nucleation, since some crystals appear to nucleate at the interface of the protein drop and the surrounding oil.

2.) Contrary to the experiment of Galkin and Vekilov, we change the protein supersaturation by changing the size of the protein drop and, by extension, the protein concentration. As the drops are quenched to a volume ⅓ to ¼ of the original volume, they begin to pin on the wall of the storage chamber; in the future a judicious choice of surfactant can reduce this problem[38]. The drops did not shrink uniformly and a thin film of protein remained on the PDMS wall. Without the use of fluorescently labeled protein it is not possible to determine the extent of this film and how much protein remains in the aqueous drop. This is a cause of error in the measurement of a) the protein supersaturation at which the crystals nucleate and b) the drop volume at those supersaturations. We can experimentally probe the extent of this error and thus the discrepancy between our and Galkin-Vekilov results by using different surfactants and varying their concentrations.

3.) The salt concentration in our experiment is not constant, while in the case of Galkin and Vekilov it remains at 2.5% throughout the duration of the experiment. This makes it difficult to compare our respective results.

4.) The supersaturation in our experiment is constantly changing during the quench. We assume that most crystals nucleate at the highest supersaturations (+/- 10%), but the time spent in this regime is short (on average 1 hour). Consequently, some nuclei may not grow large enough and will melt during the subsequent low supersaturation period. Therefore, we expect the mean number of crystals N_{exp} and hence the nucleation

rate to be small compared to that of Galkin and Vekilov, where the high supersaturation is maintained for up to twelve hours. In the future, we will use fluorescently labeled protein to obtain more information about the origin and evolution of crystals.

5.) Lastly, our assumption that the nucleus surface tension and the constants *A* and *B* are independent of the protein solubility in the range of interest could be a source of error. For example, a 10% decrease in surface tension results in an increase in nucleation rate of up to 10^6 orders of magnitude. In principle the surface tension of the protein crystal-solution interface should be measured independently.

Conclusion

We have shown that the PhaseChip is a promising device for protein crystallization, in particular for optimization of crystallization conditions. Varying the quench depth (concentration) of protein drops on-chip is a practical way to control protein supersaturation levels. The PhaseChip makes this process as convenient as changing the temperature of the test solution through the exchange of water between the protein drop and reservoir. Controlling the protein concentration in specific ways can be used to decouple nucleation from growth, as we have demonstrated by the observation that the number of crystals per drop is strongly correlated with the degree of supersaturation. This approach can be utilized to both screen hundreds of crystallization conditions simultaneously and optimize the crystal growth at a few selected conditions. This device can also be easily combined with a temperature stage, as suggested by Laval et al.[39] in order to increase the number of explored crystallization pathways.

The calculated values of nucleation parameters such as the nucleation rate and surface tension of critical nuclei in our experiment are somewhat higher than those found

by Galkin and Vekilov, but still within the range of literature results.[24,**Error! Bookmark not defined.**,25,40] We suggest that this discrepancy comes chiefly from the experimental method applied, where the supersaturation during the quench is not constant, and from the approximation of constant surface tension employed during analysis.

Future experiments will rely on the use of a better surfactant to avoid protein film formation. We will also use fluorescently labeled protein and dynamic light scattering to detect crystals earlier in order to better analyze crystallogenesis. Additionally, using non-confined spherical drops in contrast to disk-shaped confined drops will minimize protein contact with PDMS, which should lower the heterogeneous nucleation rate. Such a device could contain thousands instead of hundreds of drops and so significantly improve our statistics. We also envision modifying the discreet concentration gradient[41] employed in the current PhaseChip reservoir into a continuous gradient and using it in tandem with a temperature gradient stage, to greatly increase the number of crystallization conditions that can be screened at the same time.

Acknowledgement

The authors would like to acknowledge funding from National Institutes of Health NIH-NIGMS, STTR R41 GM083482-01. We acknowledge Jung-uk Shim's work developing the microfluidic device and thank Michael Heymann for assistance with the numerical model and Frédéric Gobeaux for helpful discussions.

Chapter 7. Mapping and Manipulating Temperature-Concentration Phase Diagrams Using Microfluidics

Šeila Selimović, Frédéric Gobeaux, Seth Fraden

(Submitted to *Lab on a Chip* 2009, reproduced by permission of the Royal Society of Chemistry.)

Abstract

We describe a microfluidic device for measuring the phase diagram of aqueous samples as a function of concentration and temperature, based on a previous device, the PhaseChip. This double-layer (poly)dimethylsiloxane (PDMS) device contains a storage layer, in which hundreds of nanoliter sized aqueous droplets can be simultaneously formed and stored. A second layer, separated by a thin, water-permeable PDMS-membrane contains twelve reservoir channels filled with different salt solutions. When there is a difference between the concentrations of salt in the reservoir solutions and the aqueous droplets, water migrates across the membrane and causes the droplets to reversibly shrink or expand. As a consequence, the concentration of all solutes inside the droplets changes. We now incorporate a temperature stage that generates a linear gradient in temperature across the chip oriented perpendicular to the concentration gradient. Robust operation of several variants of the PhaseChip are demonstrated with four examples: liquid-liquid phase separation in (I) a polyethylene glycol (PEG) – salt mixture and (II) bovine eye-lens protein (γB crystallin); protein crystallization experiments (III)

on reversibility and salvage pathways in Lysozyme from chicken egg white and (IV) on *N*-acyl-L-homoserine lactonase AiiB(S35E) from *Agrobacterium tumefaciens*.

Introduction

In the past few years there has been a concerted effort in the microfluidics community to design new tools for studying protein crystallization and the phase behavior of aqueous solutions.[45,46,47,48,49,50,51,55,56] The main advantages of microfluidic devices for these applications are a reduction in volume of the costly proteins needed to run a crystallization screen and the increased control over the physical parameters affecting phase transitions. Some devices also integrate complex functions, such as formulation[46] and allow for temporal control of the solute concentration[51] and temperature[47]. Previously, with a device we refer to as the PhaseChip[51] we have shown that manipulating the osmotic pressure of the solution is an effective way to control the solute supersaturation, for example in order to decouple crystal nucleation from crystal growth.[50,51] Temperature, however, is also a key parameter that affects supersaturation.[52,53,57] In this paper we report the capabilities of a new generation of the PhaseChip, which combines control over solute concentration with temperature control and enables us to measure the concentration and temperature dependent phase diagram of proteins and other aqueous solutions. Additionally, we can conduct hundreds of protein crystallization screens simultaneously, while still consuming a small amount of solute.

In this paper, the PhaseChip refers to a class of bi-layer (poly)dimethylsiloxane (PDMS) microfluidic devices for phase studies of polymers and proteins. In one device,

the upper layer contains over 792 aqueous droplets stored in 20 nl wells[58] (Figure 1a). Another device, designed for high throughput crystallization and phase transition experiments, can store 5,040 emulsion droplets in 65 pl wells (Figure 1b). From now on, we will refer to the two devices as the "20 nl PhaseChip" and "emulsion PhaseChip", respectively. The bottom layer of the PhaseChip is the same for both devices and contains reservoir channels through which salt solutions flow continuously (Figure 1c). The well and the reservoir layer are separated by a thin membrane of PDMS, which is only permeable to water, but not to polymer, protein or salt. As a consequence, the reservoir channels act as chemical potential reservoirs[51]. In our experiments the droplets and the reservoir solutions initially contain different concentrations of salt, and the resulting difference in chemical potential of water inside the reservoir and inside a drop drives the flow of water across the membrane. Depending on the direction of this gradient, water flows either into the drops, thereby swelling them and lowering the solute concentration, or out of the drops, therefore shrinking them and raising the solute concentration. Either process is reversible. Note that as a droplet changes size, the concentration of all solutes in it changes in the same way, so e.g. the concentrations of protein, precipitant, buffer, and polymer within the same drop are coupled. This is implicit in all phase diagrams included in this paper, even when it is not expressly stated.

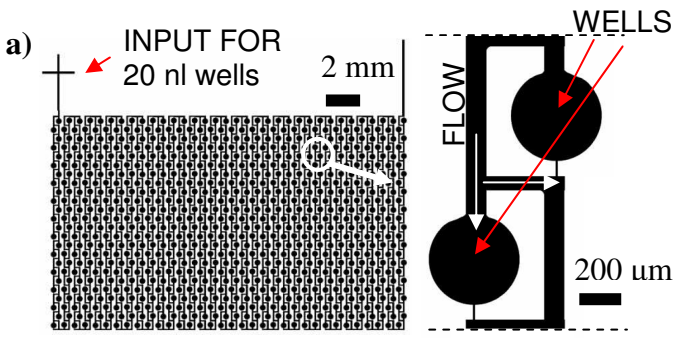

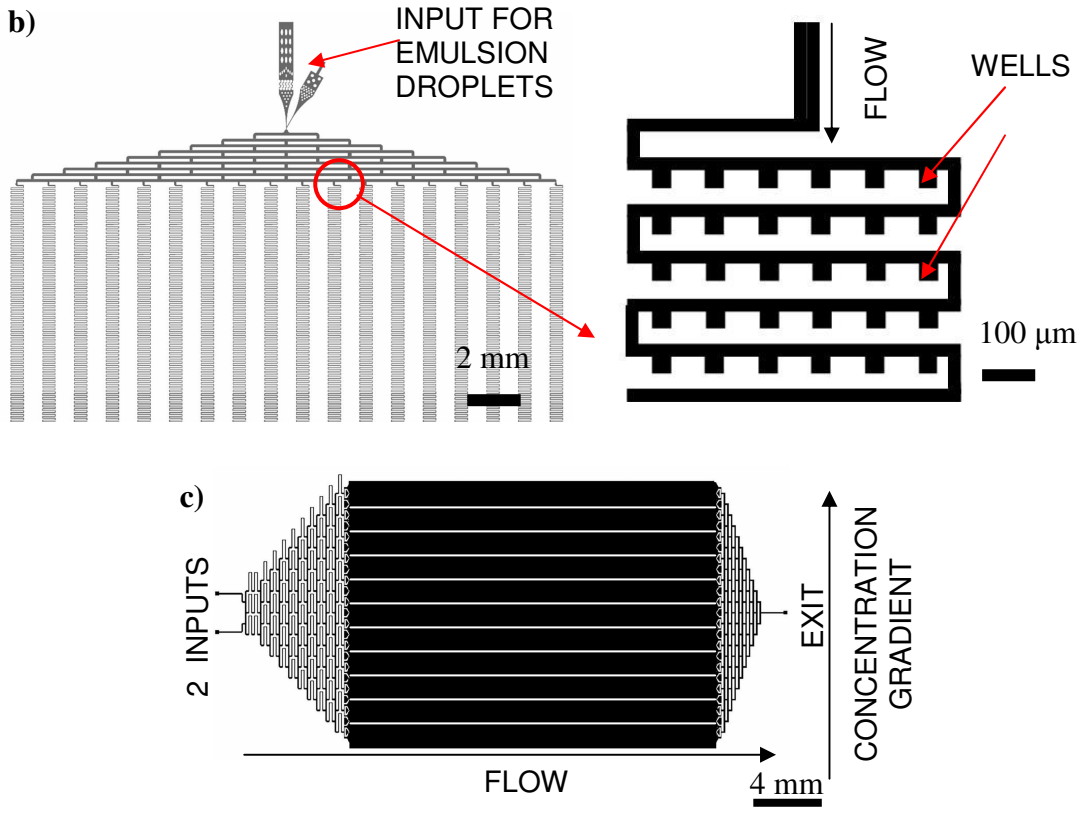

Figure 1. **(a)** Drawing of the "20 nl PhaseChip": low-resolution drawing of the storage layer and high-resolution image of a unit cell that contains two storage wells. The well diameter is 600 µm. **(b)** Drawing of the "Emulsion PhaseChip" for storing surfactant stabilized drops: low-resolution drawing of the storage layer and high-resolution image of thirty wells. Height and width of the flow channels are 50 µm, while the wells are deeper with dimensions of 50 µm x 60 µm x 70 µm (length x width x height). **(c)** Schematic of the reservoir layer used for both PhaseChip variants. Two inlets for two different salt solutions are shown on the left. As the solutions flow to the right, they mix in the triangular tree-like region on the left until they reach the main reservoir channels. Once the solutions have passed this region, they exit on the right.

The reservoir has a tree-like structure, originally developed by Jeon et al.[54]: Two fluids of different salt concentration (e.g. high concentration and low concentration salt solution) enter the reservoir independently, then as the flows branch through the tree-like channel structure, their contents mix via diffusion and finally separate into twelve distinct streams, where salt concentration varies linearly from stream to stream. There are 24 reservoir channels in total, but sets of two adjacent channels carry the same reservoir solution, generating a total of twelve discrete salt conditions. This gives rise to a one-dimensional spatial gradient of salt concentration across the reservoir channels, which in turn controls the solute concentration inside the droplets and thus generates a concentration gradient across the droplets stored on-chip. In operation, the PhaseChip is loaded with drops of identical solute concentration, eliminating the need for complex drop formulation elements. As the experiment progresses and the drops "equilibrate" with the reservoir, their concentration changes, leading to drops of high solute concentration on one side of the chip and low solute concentration on the other side (Figure 2a). Note that there is also a leakage flux of water from the drops to outside the chip. To be precise this means that the drops never equilibrate with the reservoir; instead, in steady state, a constant flux of water continuously flows from the reservoir through the drops and into the environment. Consequently the concentrations of the drop and reservoir are different.[51]

The PhaseChip also allows us to reversibly vary the solute concentrations inside the droplets by changing the concentration of the reservoir salt solutions. This affords the possibility of multiple cycles of supersaturation per sample in a closed device. Most microfluidic systems capable of regulating the solute concentration do not offer such

wide range of control: The crystallization system developed by Quake[46,55] utilizes free interface diffusion, and the approach taken by Ismagilov[45,56] relies on microbatch droplets, but neither method is reversible. Microfluidic phase and crystallization studies based on temperature quenches, like in the case of Salmon[57], are reversible, but there is no on-chip control over the solute concentrations.

In addition to this concentration control, the PhaseChip is placed on a thermal stage, in which a temperature gradient is generated by placing two independent thermoelectric coolers at opposite ends of a thin metal plate (Figure S2). The PDMS device is positioned such that the direction of the temperature gradient is perpendicular to the concentration gradient (Figure 2b). In effect, the PhaseChip now displays a two-dimensional phase diagram of the solutes in question, with each position on the chip corresponding to a particular value of concentration and temperature. Hence, any phase change observed in the droplets can be assigned quantitative values of temperature and solute concentration during the experiment. This information can then be used to readily adjust experimental parameters in order to either independently expand or reduce the temperature or concentration range.

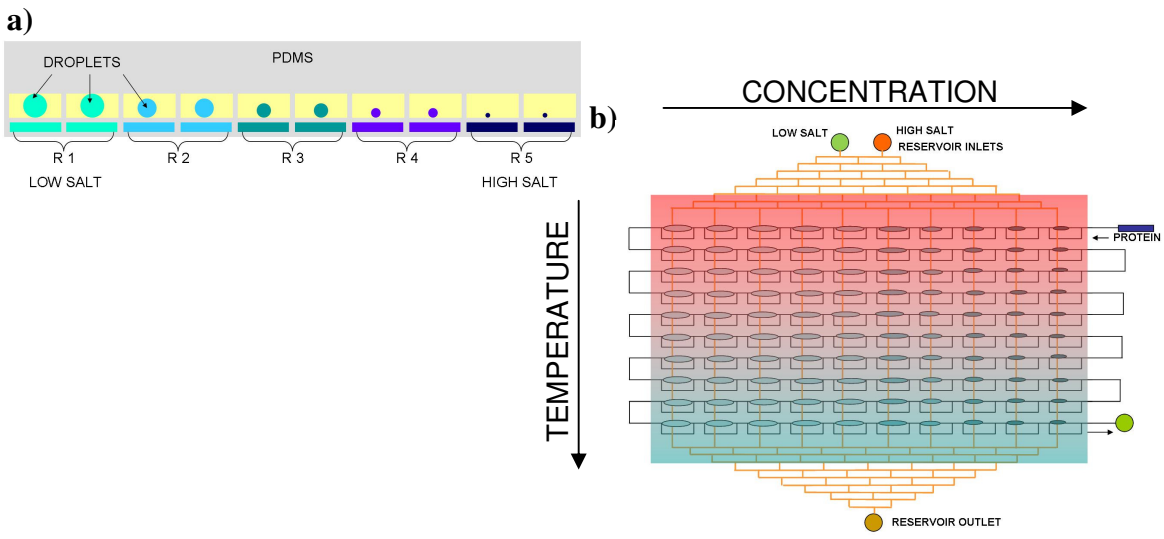

Figure 2. (a) Schematic of the PhaseChip cross-section (simplified). Five, instead of the twelve sets of reservoir channels (R1 - R5) carrying different salt solutions are shown. Each set contains two reservoir channels, such that there are two 20nl sized droplets exposed to the same reservoir solution at a particular temperature (in the case of the emulsion device, five droplets are exposed to the same reservoir solution at any given temperature). As the reservoir solution becomes saltier (from left to right), so do the droplets. This is indicated by their reduced size and deeper color (also from left to right). **(b)** Schematic of the concentration and temperature gradients on the PhaseChip. When two different salt solutions are introduced into the reservoir (LOW SALT and HIGH SALT), a discrete linear gradient of salt concentration forms across the reservoir channels (in this sketch, the salt concentration increases to the right). Originally, all droplets are identical and have the same size and solute concentrations. When the droplets (shown as blue ovals) achieve steady-state with the reservoir solution underneath, the solute concentrations inside the droplets change. In this drawing, the droplets on the left side of the chip swell (the solute concentrations decrease), and the droplets on the right side of the chip shrink (the solute concentrations increase). This is indicated in the image by the lighter blue color and larger size of the drops on the left and the deeper blue and smaller size of the droplets on the right. Superposed on the concentration gradient is a continuous linear temperature gradient, indicated in the drawing as a colored rectangle that changes color from blue (low temperature) to red (high temperature). Directions of both gradients are reversible. (Online in color.)

Experimental Section

The two versions of the PhaseChip (Sylgard 184 PDMS, Dow Corning) described here can either store 816 aqueous drops of 20 nl volume ("20 nl PhaseChip"), or 12000 emulsion drops of 65 pl ("emulsion PhaseChip") in individual wells. The complete storage region is 2 cm × 4 cm in size for both PhaseChip devices. The oil is pumped constantly through the storage region at 10 µl/hr in order to compensate for the change in volume as the drops shrink. In both PhaseChip designs the drops are separated by fluorinated oil, such that they are physically and chemically isolated from each other and represent independent experiments. Details of PhaseChip manufacture are in the supplement.

The larger droplets of 20 nl are formed via the "store, then create" method we described previously[58], where a long plug of aqueous solution is first stored in the wells and then separated into distinct droplets. The advantages of the "store, then create" method are zero dead volume and the elimination of the need for complex drop formation elements such as nozzles. Typically the 20nl PhaseChip consumes less than 2µl of solution. The carrier fluid in this case is either a mixture of fluorinated oil FC-43 (Acros) and 12% v/v of 1H,1H,2H-2H-Perfluoro-1-Octanol surfactant (Fluka) in protein experiments, or FC-43 alone in polymer experiments. In contrast, the emulsion droplets are formed in a separate PDMS device using a 50 µm wide nozzle[51]. Emulsion droplets are then stored for up to several days in a glass vial, until they are used in an experiment. During this time, no stability or adhesion problems occur, due to the presence of the surfactant. Next, emulsion droplets are injected into the emulsion PhaseChip via polytetrafluoroethylene (PTFE) tubing. Surface tension forces guide the drops into the

wells[51]. Here, the carrier fluid is a partially fluorinated oil, 2-trifluoromethyl-3-ethoxydecafluoro hexane (HFE 7500, 3M Novec) with 2% w/w of a proprietary non-ionic triblock surfactant kindly provided by RainDance Technology and similar to the one synthesized by Holtze et al[59]. In any given experiment more than 90% of wells are filled with a single protein or polymer drop and all stored drops have the same initial composition.

The temperature stage is fabricated from brass, with two embedded thermoelectric coolers (TEC, Melcor PT4-7-30) that can be controlled independently by two PID circuits (Analog Devices, EVAL-ADN8831). These are in turn operated via a LabView interface, thereby allowing us to create a temperature gradient across the long side of the PhaseChip storage region (Supplementary Figure S2). On this concentration - temperature gradient grid, where the two control parameters are perpendicular to each other, several droplets are exposed to the same combination of concentration and temperature. This is because our reservoir design is limited to twelve different concentrations per chip. However, the number of different temperatures is set by the number of storage rows, which is 33 for the 20nl-chip and 90 for the emulsion chip, as shown in Figure 1. In particular, two 20-nl sized droplets, or 5 emulsion droplets are exposed to the same pair of concentration - temperature conditions. While there are several hundred distinct and simultaneous experiments on each version of the PhaseChip (396 and 1080 for the 20nl and emulsion chips, respectively), the built-in redundancy in physical conditions serves to check the reproducibility of the phase behavior.

In all the experiments we describe the drops initially introduced into the PhaseChip are identical. During the loading of drops into storage wells all reservoir

channels are filled with a salt solution whose concentration matches the salt concentration inside the drops. This prevents the concentration of solutes in the drops from changing before the experiment begins. After the drops are loaded, concentration gradients across the chip can be generated by flowing two different salt solutions through the reservoir layer. Temperature gradients across the chip can be generated by setting the TECs to different temperatures. Typically it takes twelve hours for the drops to reach a steady-state concentration and two minutes to reach a steady state in temperature.

Once all drops are loaded into the PhaseChip, the device is placed on an automated 3-axis microscope stage with a 4x objective lens and a resolution of 10 μm. We periodically record images of the aqueous drops, typically every 15 minutes. This allows us to measure the size of the drops and thus determine changes in solute concentrations over time and also to record any phase changes[51]. The volume of the drops and shape of the 20 nl wells are such that the drops take on a disk-like shape inside the storage wells, and the height of the drops remains constant at all times. Hence, the change in drop volume only depends on the change in drop area, which we measure using image recognition software (NI Vision Assistant). Protein, polymer and salt concentration in a drop at time t is then obtained from the drop area $A(t)$, the initial area A_0, and the known initial concentration C_0 : $C_0/C(t) = A(t)/A_0$. The emulsion droplets, on the contrary, are spherical throughout the experiment. In this case we measure the drop radius, rather than the drop area, and then calculate the drop volume and deduce the solute concentrations as a function of time. We conduct these measurements to create precise temperature - solute concentration phase diagrams. One of the attractive features of the PhaseChip, however,

is that a two-dimensional grid with distinct phases can be visualized directly on-chip with a microscope, even before the images are evaluated.

We demonstrate the operation of the PhaseChip in four examples: I) polymer-salt liquid-liquid coexistence curve, II) eye-lens protein liquid-liquid coexistence, III) protein crystallization with Lysozyme and IV) protein crystallization with a quorum-quenching protein AiiB(S35E).

I) Polymer-salt coexistence: polyethylene glycol (PEG) – ammonium sulfate $(NH_4)_2SO_4$

We determine the concentration-temperature phase diagram of the water soluble polymer PEG 22 kDa in the presence of ammonium sulfate salt ($(NH_4)_2SO_4$) in a molar concentration ratio of 1:29.5. Three experiments were done using 20 nl drops to test whether or not the final state depends on the thermodynamic path taken from the initial state. The droplets contain 14.5 mM PEG (Sigma), 427 mM ammonium sulfate (Fisher) and Hannaford blue food dye (5% by volume) at the beginning of each experiment. The polymer solution is prepared and filtered off-chip (0.2 μm syringe filter, Corning, product number 431212), as are the buffers and salt solutions. As the drops shrink the concentrations of PEG and salt grow, but the ratio remains constant at 1:29.5. We record the state of the droplets (single phase or liquid-liquid phase separated) at various temperatures and concentrations. We further conduct two experiments with 65 pl emulsion droplets to determine whether the phase diagram shows a dependence on the drop volume.

a) 20 nl droplets at 14.5 mM PEG (22kDa) and 427 mM ammonium sulfate are stored in the "20 nl PhaseChip" and subjected to a concentration gradient between 215 mM and 1.33 M ammonium sulfate. The temperature is kept constant at 10°C across the PhaseChip until the droplets have equilibrated with the reservoir solutions underneath. The temperature is then incrementally increased from 10°C to 40°C in steps of 5°C every 2 hours, and finally reduced to 10°C in the same fashion.

b) 20 nl droplets at 14.5 mM PEG (22kDa) and 427 mM ammonium sulfate are stored in the "20 nl PhaseChip" at 8°C, and a temperature gradient between 8°C and 40°C is then applied across the chip. After 15 minutes, a period sufficient for the droplets to equilibrate in temperature, a concentration gradient through the reservoir channels is applied as described in the previous experiment and maintained for an equilibration period of 24 hours.

c) 20 nl droplets containing 9.67 mM PEG (22kDa) and 285 mM ammonium sulfate, again in a ratio of 1:29.5, are stored in the "20 nl PhaseChip" at 20°C, but this time the concentration and temperature gradients (5°C to 38°C) are applied simultaneously. The temperature gradient is chosen such that the difference in temperature between two adjacent drops along the temperature axis is roughly 1°C.

d) 65 pl emulsion stabilized droplets used in this experiment contain 14.5 mM PEG 22 kDa and 427 mM ammonium sulfate (a ratio of 1:29.5), but no dye. We introduce 0.5M and 4M ammonium sulfate solutions into the reservoir in order to regulate the concentration of solutes in the drops. The experiment is conducted at room temperature.

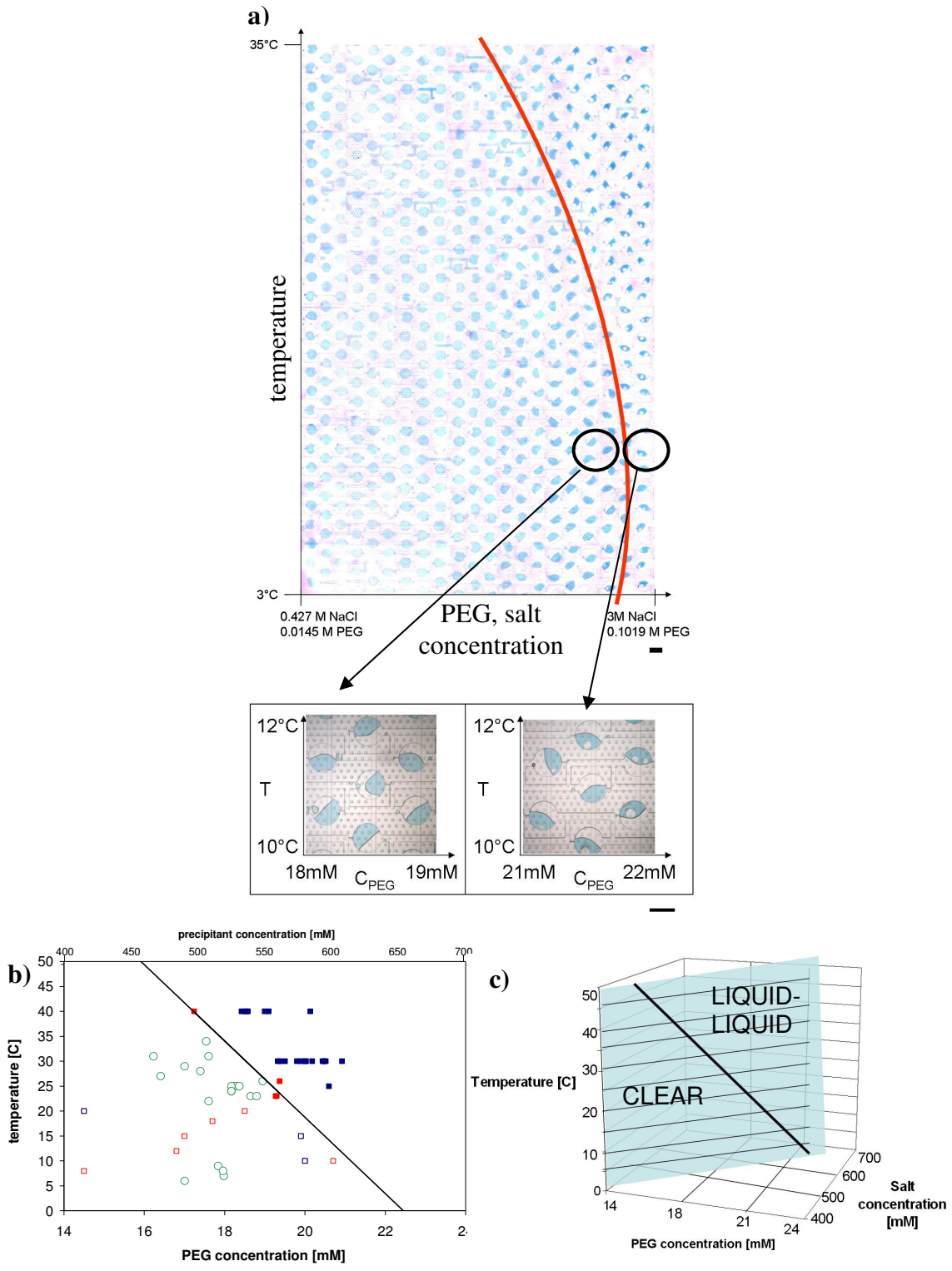

Figure 3. (a) Stitched image of the PhaseChip (630 droplets are shown). The droplets contain a mixture of PEG 22kDa, $(NH_4)_2SO_4$, and blue dye for easier visualization. The

axes indicate the applied concentration and temperature range, but not all drops have equilibrated with the applied reservoir concentrations at this time, hence the PEG and salt concentration labels on the concentration axis in this image do not reflect the actual solute concentrations inside the drops. The solid red line serves as visual aid to distinguish the regions of clear drops (left of the curve) and liquid-liquid phase separated drops (right of the curve). The shown area is 1.8 mm x 3.8 mm. (For a higher-resolution image see Supplementary Figure S3.) Magnified images of clear (left) and phase separated (right) droplets in the PhaseChip are shown below. The labeled concentrations are actual measured solute concentrations inside the drops. Clear drops: C=18 +- 0.05 mM PEG, T:10°-12°C. Phase separated drops: C=22 +- 0.05 mM PEG; T:10°-12°C. Scale bar is 600 μm. **(b)** Phase diagram for PEG 22kDa and ammonium sulfate in the ratio of 1:29.5. Open symbols denote clear drops from all three experiments and filled symbols denote phase separated drops from experiments a) and b). Blue squares denote results from experiment a), red symbols are from experiment b). Green circles denote single phase drops from experiment c). The solid black line is the phase boundary. Note that the PEG and salt concentrations in the droplets are coupled. **(c)** 3D representation of the phase boundary shown in (c). (Online in color.)

Results:

Experiments I a), b), c): A view of the PhaseChip with a clear and a liquid-liquid phase-separated region can be seen in Figure 3a. The red curve serves as a guide to the eye: the blue droplets to the left of it are large and clear, while the drops to the right of the curve are much smaller (because concentrated) and phase separated. Two examples of

drops from either side of the red curve are also shown. Concentration-temperature data from all three experiments conducted on the PEG - ammonium sulfate mixture are reported in Figure 3b. The three sets of results match each other, resulting in a phase boundary (solid black line) that divides clear droplets from liquid-liquid phase separated droplets. Thus, it is irrelevant which parameter, concentration or temperature, is adjusted first. A path-independent final state is indicative of an equilibrium phase transition. Once the droplets phase separate into two distinct liquid phases (a polymer-rich and a salt-rich phase), we are unable to determine the concentration of salt and polymer in each phase simply by measuring the volume of the drops. This means that we can determine the phase boundary, but not the composition of the co-existing phases.

Experiment I d): In the emulsion experiment we detect the onset of liquid-liquid phase separation at 18mM $(NH_4)_2SO_4$, a concentration value that is comparable to our measurement made on 20 nl drops at room temperature (19 mM). Figure 4 displays a series of droplets along the concentration gradient. As the two phases separate, the difference in surface tension between them leads to the formation of PEG-rich satellite droplets. (When food dye, which partitions into the salt-rich phase, is used in these experiments, the large droplets turn blue, indicating that the satellite droplets contain a PEG-rich phase.) Such a satellite droplet never detaches completely nor do drops coalesce when they come into contact. We speculate that this is due to the surfactant, which stabilizes the emulsion.

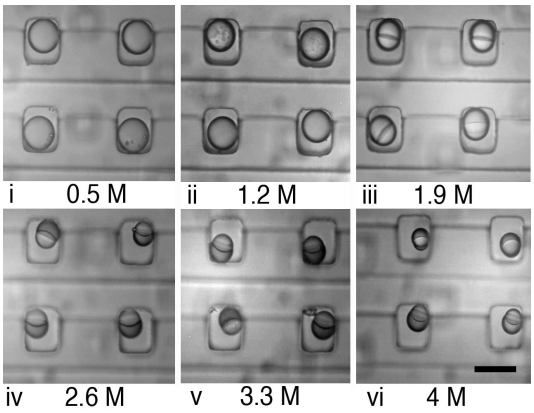

Figure 4. Equilibrium phase separation in emulsion droplets containing a mixture of PEG and $(NH_4)_2SO_4$ is shown at different positions along the concentration gradient in the PhaseChip, at room temperature. The concentration of the corresponding reservoir solution is indicated in each image and the concentration of both PEG and ammonium sulfate increases from (i) to (vi). Scale bar is 60 μm.

II) Liquid-liquid phase separation in protein: Bovine γB crystallin

Crystallins are water-soluble proteins in the eye lens, where they help to increase the refractive index without scattering light, thereby making an optically transparent lens. With advanced age, proteins that are damaged tend to phase separate within each cell. The resulting heterogeneity (cataract) scatters light, rendering the lens opaque.[60,61,62] We use the PhaseChip to demonstrate the ability of bovine γB crystallin to undergo liquid-liquid phase separation in response to changes in temperature and concentration.

The protein sample used in our experiment originally contains 96.5 mg/ml γB crystallin in D_2O ; 50 mM sodium phosphate and 20 mM dithiothreitol at pH 7.1. The choice of D_2O as solvent, together with dithiothreitol, puts the phase separation into a convenient temperature range for our PhaseChip experiments, while at the same time

inhibiting a slow oxidation of γB crystallin that can, with time, bias the determination of the phase boundary. The reservoir solutions are pure water and 400 mM sodium phosphate. The temperature gradient originally spans 1°C to 22°C, and is later reduced to a range between 12°C and 18°C.

Results:

At the initial concentration, the protein phase separates at 6.5°C. At higher concentrations the boundary occurs at progressively higher temperatures. Figure 6a shows an image of the PhaseChip 20 hours after the start of the experiment, with temperature (in °C) and concentration (mg/ml) ranges indicated along the arrows. At this time the droplets have not yet equilibrated in concentration with the reservoir solutions. The dashed line demarcates the phase boundary. At temperatures above the boundary the drops appear clear, indicating the presence of a single phase solution. At temperatures below the boundary the protein droplets begin to undergo liquid-liquid phase separation and thus appear dark. Under high magnification one observes tiny globules of a gel. The interpretation is that the solution starts to bulk phase separate into coexisting liquid-liquid phases, but is kinetically arrested on the high concentration end by the intervention of gelation[63,64]. Magnified images of the PhaseChip at two different conditions are included in Figure 6b, to make the distinction explicit between clear and phase-separated drops.

After the solute concentration in the droplets has further increased, we reduce the width of the temperature gradient to a range between 12°C and 18°C across the full length of the drop storage region. Then the temperature difference between two adjacent drops along the temperature gradient is only 0.2°C, allowing us to determine more

precisely the position of the phase boundary. The resulting images of the PhaseChip can be seen in Figure S4. We note that although the range of measured concentrations and imposed temperatures on the PhaseChip changes throughout the experiment, and thus the phase boundary moves on-chip, its absolute position remains constant, i.e. it is always measured at the same values of concentration and temperature. In other words, all droplets are at equilibrium at any given time, because any phase change in the droplets occurs faster than the change in solute concentration. The equilibrium, however, shifts on-chip throughout the experiment, and the protein solution is in a quasi-equilibrium state. The resulting data is shown in Figure 6c: We measure the temperature, precipitant and protein concentrations at which the phase boundary occurs at different times in the experiment (at t=20, 51, and 69 hours). As the drops continue to shrink, however, the range of solute concentrations accessible on the PhaseChip changes, such that at each point in time we access a different part of the global phase boundary. (Corresponding images of the PhaseChip are included in the Supplementary Figure S4.)

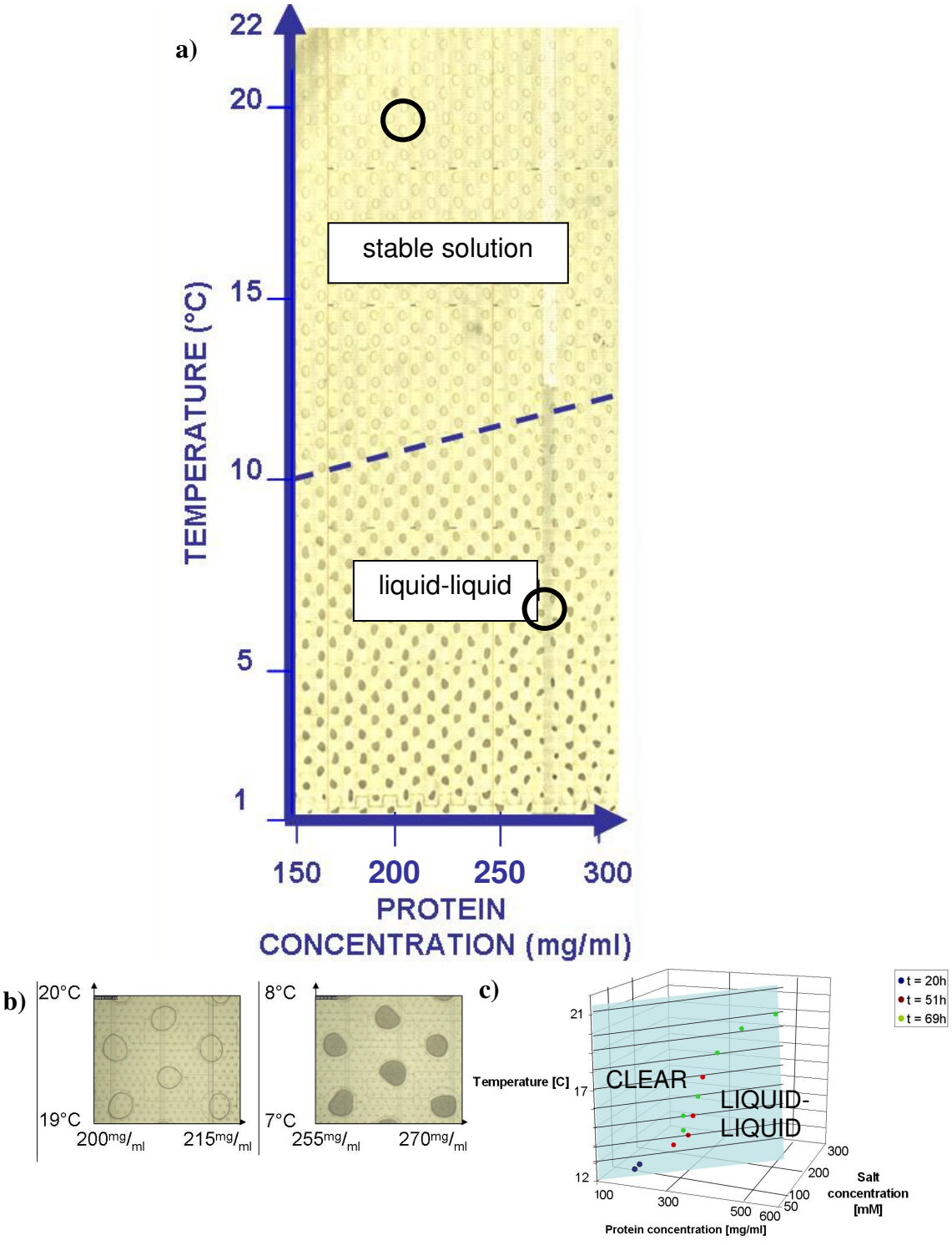

Figure 6. **(a)** Photograph of the PhaseChip 20 hours after the start of the experiment. The dashed line demarcates the phase boundary between single phase and liquid-liquid phase

separated regions. **(b)** Magnified images of two sets of protein droplets, marked with circles in a). Left: clear droplets (20°C, 200mg/ml γB crystalllin). Right: turbid droplets (8°C, 270mg/ml γB crystalllin). **(c)** Phase boundary of γB crystalllin, assembled from data accessible at different times throughout the experiment.

III) Studying phase separation and salvage pathways in a Lysozyme - PEG mixture using emulsion droplets

The goal of this experiment is to evaluate the reversibility of phase changes in the protein sample and probe different salvage pathways[67]. We use a mixture of 16.5 mg/ml Lysozyme (Sigma, product number L7651), 2.5% w/v NaCl (Fisher) and 6.25% w/v PEG 8kDa (Sigma), dissolved in 0.05 M NaAc buffer at pH 4.8. The concentration gradient in the reservoir first spans a range from pure water (0 M NaCl) to 1.4 M NaCl, then later a range between 2 M NaCl and pure water, such that in the second step the direction of the concentration gradient is reversed. The temperature is initially set to 20°C in order to prevent premature phase separation and is constant across the chip. After the droplets have equilibrated with the reservoir (ten hours after the start of the experiment), the temperature is briefly decreased to 0°C, then increased to 25°C in 2°C steps. Then, we invert the concentration gradient by switching the two reservoir solution inputs as described above, and after a second equilibration time at 25°C the temperature is again reduced to 0°C (Figure 5a).

Results:

The temperature and concentration profiles in this experiment are shown in Figure 5a: We establish a concentration and temperature gradient, observe the phase behavior, then invert both gradients to explore the reversibility of the phase changes in the droplets. The PhaseChip allows us to conduct many experiments in the concentration - temperature space simultaneously, and the approach taken here lets us explore the phase diagram of the Lysozyme-PEG mixture until we observe crystals in some of the drops, indicating the kinetic pathways and concentration-temperature conditions appropriate for protein crystallization.

All droplets are initially clear. As the solute concentration increases to 20 - 50 mg/ml Lysozyme, the droplets become cloudy and develop a gel-like phase below 5°C,[63] but remain clear at higher temperatures. At higher concentrations (60 - 70 mg/ml) and 5°C the droplets are still cloudy, but when the temperature is further reduced (to 0°C), the cloudy phase clears up until crystals are observed (see Figure 5a and Supplementary Movie SM1). A section of the PhaseChip with 40 such emulsion droplets is shown in Figure 5c. This image indicates that a protein supersaturation level necessary for crystal nucleation has been reached in all 40 droplets, hence the chip offers results that are statistically meaningful. Drops that are kept at a low temperature (0°C), but also low concentration (25 mg/ml Lysozyme), however, exhibit different behavior: here the gel phase does not clear up, indicating that the protein is not concentrated enough to facilitate crystal nucleation and growth. These observations suggest that the phase transition from single phase to gel is reversible, but that the protein solution is not in equilibrium due to the crystal nucleation barrier. We further note that a droplet containing cloudy phase

rather than a protein crystal does not have to be abandoned in the crystallization process, but can be salvaged by controlling the concentration and temperature of the protein on the PhaseChip.

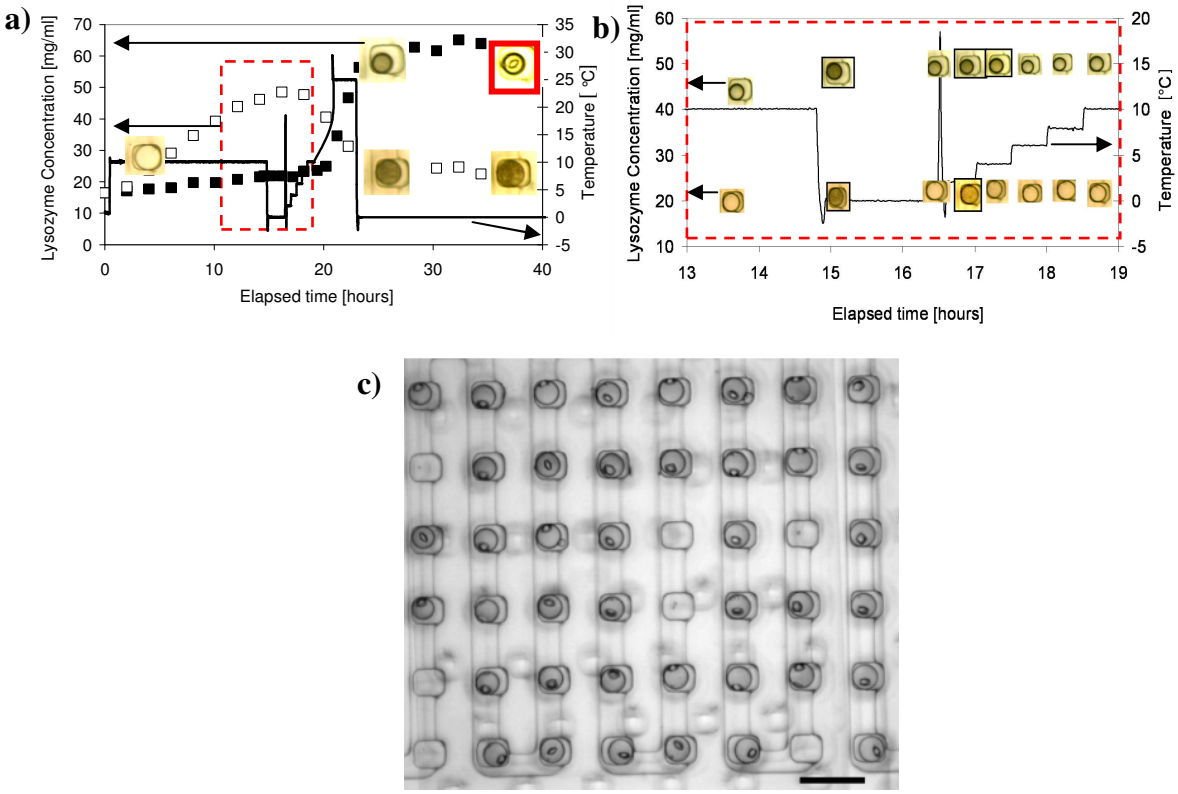

Figure 5. **(a)** Temperature - concentration profiles of two populations of droplets (open and closed icons), which are subjected to two opposite concentration gradients (from 1 to 21 hours and 21 to 40 hours). The temperature profile is the same for all droplets (full black line), but their concentrations vary relative to each other and as a function of time. The inset photographs show typical drops for the concentration corresponding to their position in the figure. The temperature is indicated by the value of the black line at the corresponding time. For example, the upper right most drop (containing a crystal) has a concentration of 58 mg/ml and a temperature of 0°C. Different phases in the droplets are

observed: clear (t=0), dark (gel phase), clear drop with a tetragonal Lysozyme crystal. **(b)** This diagram is a magnified version of the dashed red rectangle shown in (a). The position of the photographs indicates their concentration at a given time. The corresponding temperature is given by the solid line. At temperatures below 4°C the droplets become darker indicating the formation of a liquid-liquid phase separation or a gel. (Images containing gels are surrounded by a dark border.) **(c)** An area of the PhaseChip filled with emulsion droplets. The kinetic path and concentration - temperature data for this set of drops is shown in Figure a) and represented by the drop containing a crystal (the image surrounded by a red frame). Each drop contains exactly one tetragonal Lysozyme crystal. Scale bar: 120 μm. (Online in color.)

IV) Screening protein crystallization conditions for *N*-acyl-L-homoserine lactonase AiiB(S35E)

The protein drops used in our PhaseChip experiment are formulated by mixing the following components in a 1:1 ratio: 10mg/ml protein in 20mM 4-(2-hydroxyethyl)-1-piperazineethanesulfonic acid (HEPES) at pH 7.5 and 1.1 M ammonium tartrate ($(NH_4)_2C_4H_4O_6$) at pH 7.5. To control the solute concentration inside the drops we introduce two ammonium tartrate solutions in the gradient reservoir, at 0.5 M and 1.5 M concentrations. A temperature gradient is imposed simultaneously, and spans a range from 12°C to 31°C.

Results:

The *N*-acyl-L-homoserine lactonases (AHL lactonase) are enzymes that block bacterial cell-cell communication[65]. An AHL lactonase from *Agrobacterium tumefaciens*, AiiB, has been crystallized and its structure determined. The active site of the wild type AiiB enzyme has been inadvertently occupied, however, and blocked by phosphate, which is a major component in the known crystallization condition.[66] In order to observe the intact active site in crystal structure, extensive crystallization trials were carried out to search for another crystallization condition that does not contain phosphate. Here we report a crystallization condition without phosphate for a mutant protein AiiB(S35E) in which the residue serine 35 has been mutated to a glutamate. Previous crystallization tests[66] conducted in crystallization plates on microliter sized drops determined conditions that yield many crystals. The PhaseChip consumes 1000 times less protein per crystallization trial, however, making it possible to conduct more trials and scan a wider concentration and temperature space than previously possible in order to find the condition appropriate for growing a single large crystal per drop.

First protein crystals under the PhaseChip conditions described in the experimental section are observed after a period of 24 hours. Visual inspection of the PhaseChip indicates clearly delineated regions of the device that contain clear (stable) drops, drops in which the protein and precipitant have undergone liquid-liquid phase separation, and a wide crystallization region (Figure 7a). We note that there are two crystal morphologies present (elongated and compact, which we did not characterize further) and a distinct region on-chip where each drop contains exactly one crystal. The corresponding phase diagram is shown in Figure 7b.

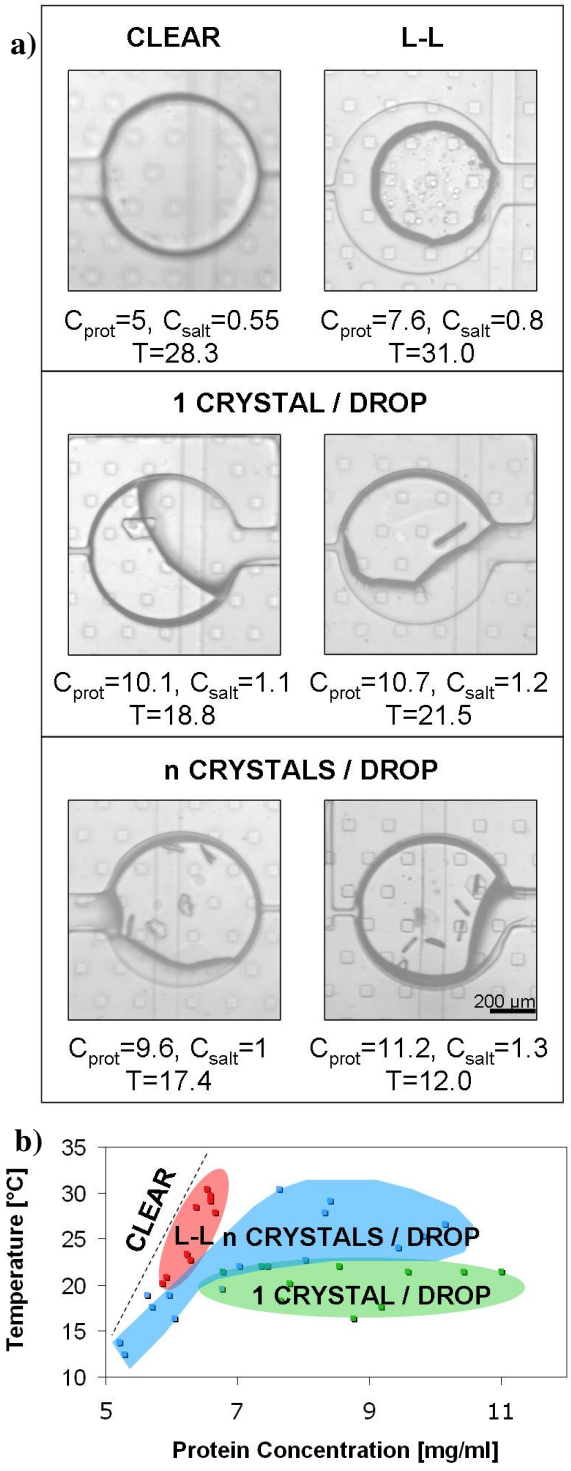

Figure 7. **(a)** Sample images from the AiiB crystallization screen, taken 31 hours after begin of the experiment. Different phases are observed: clear (single-phase), liquid-liquid

(L-L) phase separation, single crystal per drop (with two crystal morphologies) and several crystals per drop. Scale bar is 200 μm. Salt concentration (C_{salt}) is reported in mM, protein concentration (C_{prot}) is reported in mg/ml, and temperature (T) is reported in °C. **(b)** Phase diagram of the bacterial lactonase AiiB. Note that we only report the protein concentration, but it is coupled with the salt concentration. Four distinct regions are apparent in this diagram: to the left of the dashed line, the drops are stable and remain clear. Red denotes the liquid-liquid phase separated region (L-L), green denotes the region of one crystal per drop and blue denotes the region in which drops have more than one crystal on average (usually four to five). The data points shown for each region have been collected at t=31 hours. (Online in color.)

CONCLUSION

We have demonstrated the versatility of the PhaseChip for the quantitative mapping of phase diagrams and for the kinetic manipulation of thermodynamic variables to influence phase behavior. In a typical experiment, the PhaseChip consumes 2 μl of solution and controls simultaneously up to 1000 different conditions in the concentration - temperature plane. The PhaseChip offers excellent and reversible control over the concentration of all solutes inside test droplets for a range of droplet sizes, from emulsion droplets of 0.065 nl to microdroplets of 20 nl. Typically concentrations across a chip vary between a factor of 2 (Figure 6a) to 8 (Figure 4b). Thermoelectric coolers provide excellent spatial and temporal control of temperature across the full device and the PhaseChip performs equally reliably whether the temperature across the chip is constant

or a large spatial temperature gradient is applied, for example in the range of 2°C to 40°C.

We dynamically follow the progression of concentration changes in all drops stored on-chip. Thus, a visual inspection of the droplets with a microscope allows us to quantitatively evaluate an experiment before its completion, and adjust the experimental parameters to achieve a desired temperature and concentration range on-chip. This feed-back control, combined with reversible regulation of both concentration and temperature is, to our knowledge, novel in the area of high throughput microfluidic devices, and especially in microfluidics based protein crystallization.

The performed experiments demonstrate that the PhaseChip can be used to study a variety of problems, from quantitative determination of liquid-liquid phase diagrams in both polymer and protein solutions to protein crystallization screens. In the case of Lysozyme we have shown that phase changes from single phase solutions to liquid-liquid or gel phases are reversible, and we determined a salvage pathway that yielded protein crystals in 40 out of 40 droplets exposed to the crystallization condition[67]. This is an advantage over other microfluidic crystallization platforms that do no allow reversibility in temperature and concentration[45,46]. Furthermore, when studying the protein AiiB(S35E) we have shown that a concentration-temperature crystallization screen led to an optimal condition that yields exactly one large crystal per drop, rather than many small ones. This is particularly of interest to crystallographers, who rely on large and well-ordered crystals to extract structural data.

Acknowledgments

We thank Ryan Whelan, who designed and built the temperature stage; Professor George Thurston (Physics Department, Rochester Institute of Technology), who provided us with purified bovine γB crystallin samples; Dr. Walter Fast and Dr. Pei W. Thomas (University of Texas, Austin), who supplied the AiiB protein samples and Dr. Dali Liu (Brandeis University), who conducted AiiB off-chip crystallization trials. We are also grateful to RainDance Technologies, for providing us with the non-ionic triblock surfactant necessary for emulsion experiments. We acknowledge support from the Brandeis NSF MRSEC - 0820492 and from NSF IDBR - 0754769.

SUPPLEMENTARY MATERIALS

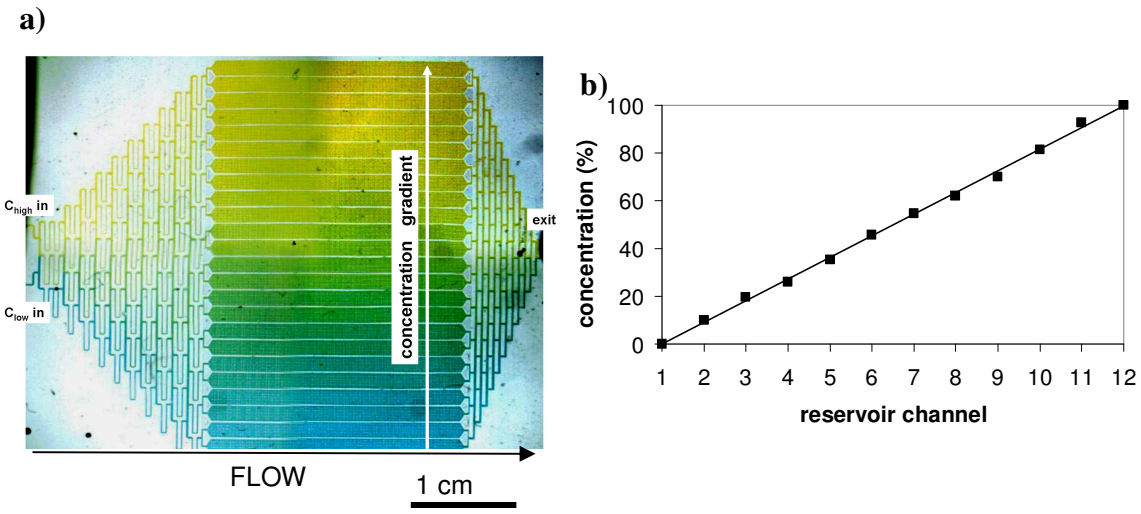

Figure S1. (a) Linear concentration gradient in the reservoir channels visualized with yellow and blue dyes (highly concentrated NaCl solution and pure water, respectively). The direction of the gradient is perpendicular to the flow direction. **(b)** Linear concentration profile of fluorescent dye in aqueous streams across twelve reservoir channels (■). The solid line is a linear fit to the data. The two aqueous solutions used in this experiment are pure water and water carrying Alexa 488 fluorescent dye. Photographs of the mixing streams were analyzed using ImageJ software (http://rsbweb.nih.gov/ij/).

a)

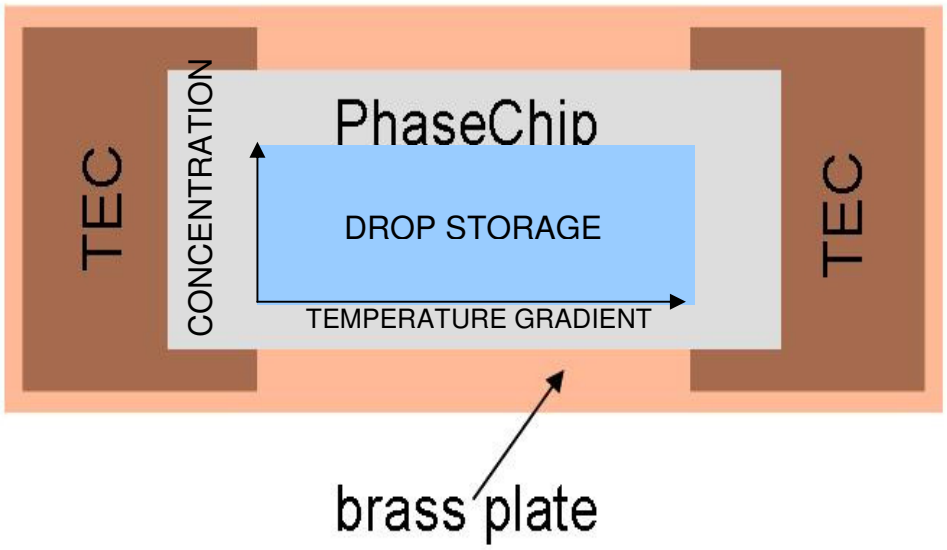

b)

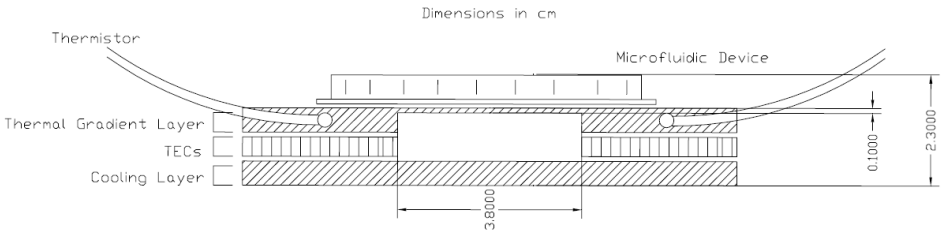

Figure S2. Thermal stage. **(a)** Top view. The microfluidic device is placed on the top of a 1 mm thin brass plate, which in turn is in contact with two thermoelectric coolers (TEC) placed on each end. Water circulates through the brass cooling layer and acts as a source / sink for heat to / from the microfluidic device. Generating a temperature gradient from 2°C to 40°C requires about 20W of power. **(b)** Cross-sectional view.

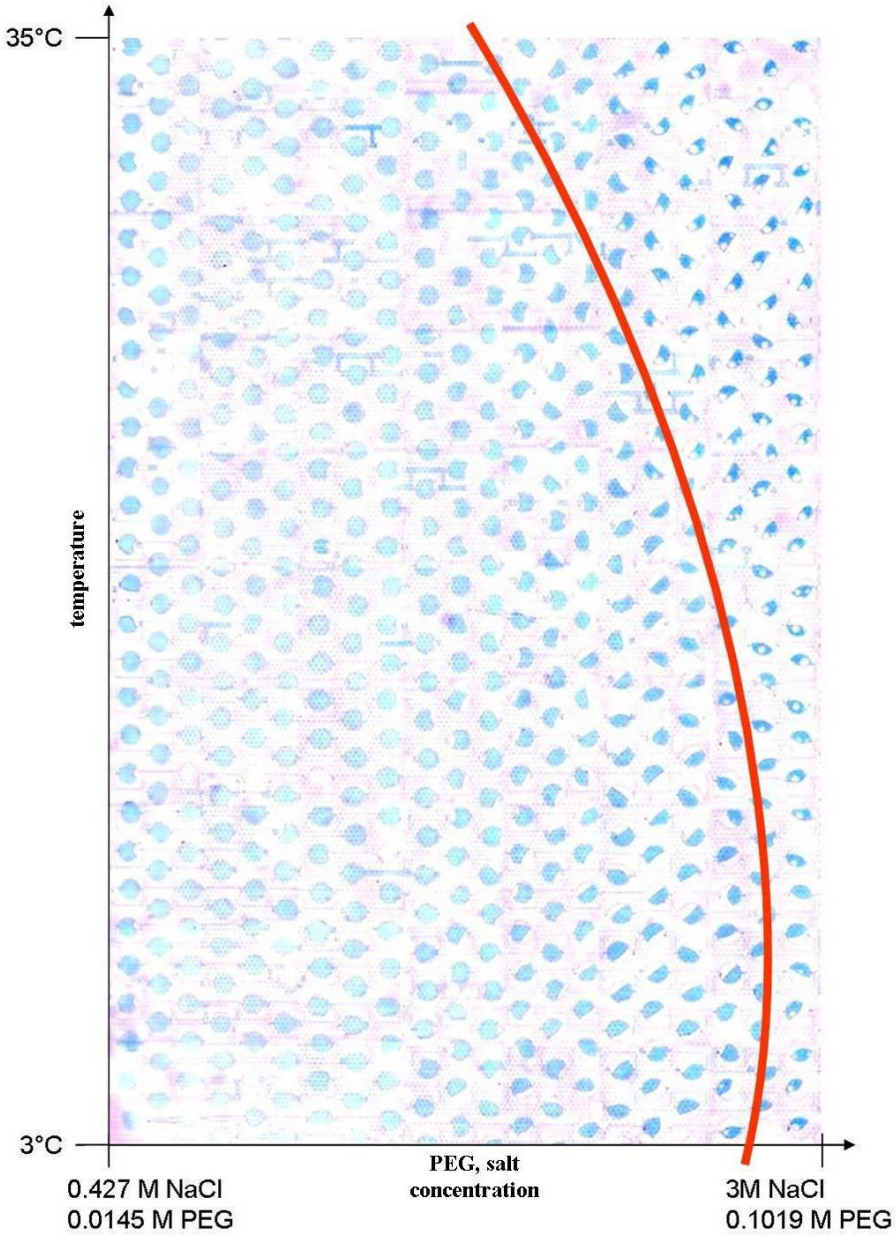

Figure S3. Magnified image of the PhaseChip shown in Figure 1a.

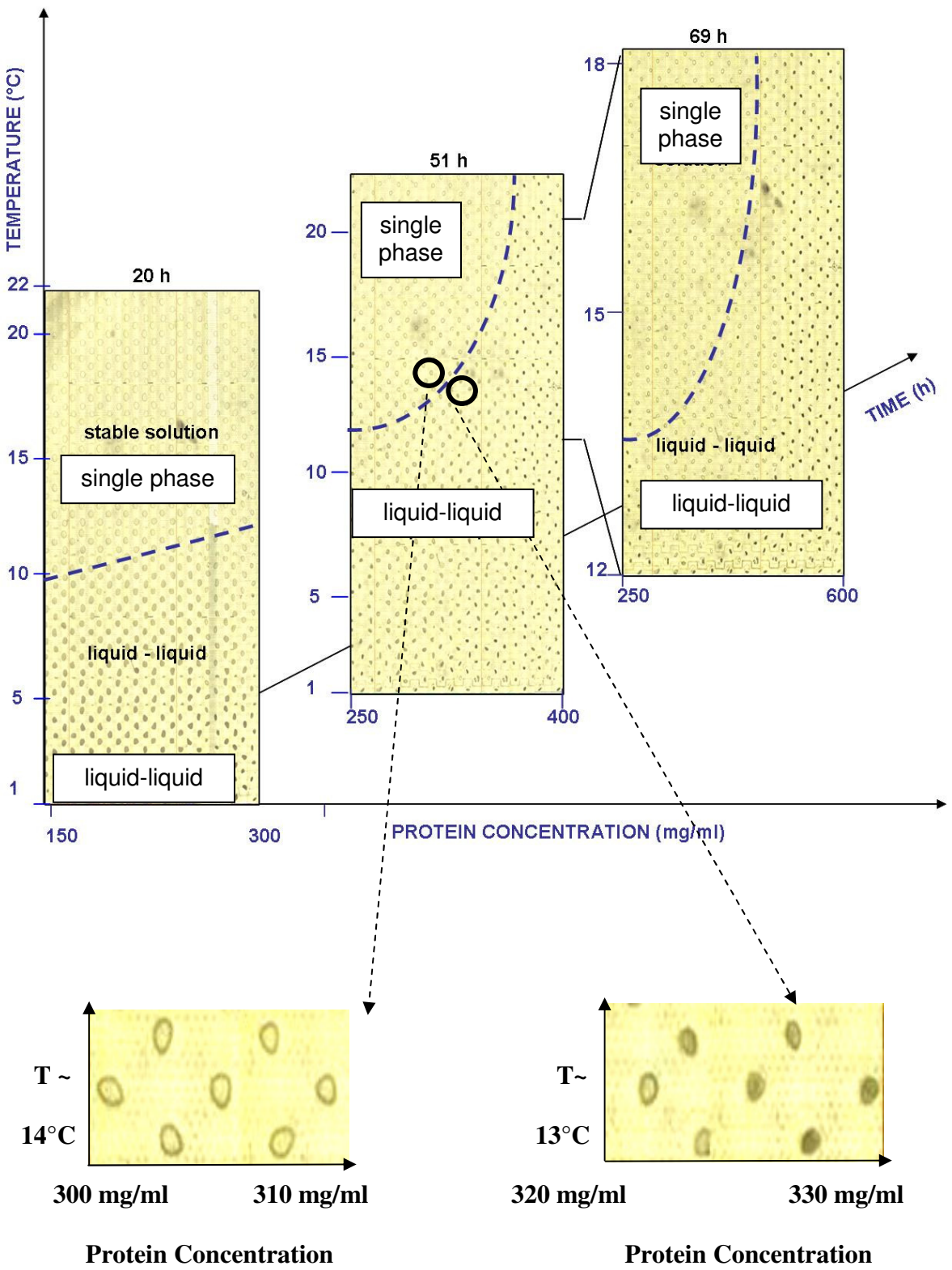
TEMPERATURE (°C)
20 h
22
20
15
10
5
1
stable solution
single phase
liquid - liquid
liquid-liquid
150
300
51 h
20
15
10
5
1
single phase
liquid-liquid
250
400
69 h
18
15
12
single phase
liquid - liquid
liquid-liquid
250
600
TIME (h)
PROTEIN CONCENTRATION (mg/ml)
T ~
14°C
300 mg/ml
310 mg/ml
Protein Concentration
T~
13°C
320 mg/ml
330 mg/ml
Protein Concentration

Figure S4. Three images of a single PhaseChip filled with 20 nl droplets of γB crystallin, taken at times t=20, t=51 and t=69 hours after the start of the experiment. The range of protein concentrations (in mg/ml) and temperatures (in °C) accessible in the experiment, as well as the phase boundary (dashed blue line) are indicated individually in each image. (The phase boundary has been determined after careful analysis of high resolution images and is more difficult to recognize in the above views of the full PhaseChip.) Note that although the phase boundary shifts in space throughout the experiment, its absolute position in terms of concentration and temperature values remains constant.

PhaseChip Fabrication Protocol

Master fabrication:

Reservoir layer:

1.) 3" silicon wafers (Silicon Sense, Inc.) are used as is, there is no need for cleaning or pretreatment.

2.) Wafers are coated with 1 -2 ml of SU8-2025 photoresist. The spin rate is first increased from 0 to 500 rpm, where it remains for 5 seconds. In this step the resist is spread on the whole wafer. Then the spin rate is increased to 2800 rpm for 30 seconds to achieve a resist thickness of 30 μm.

3.) The wafers are soft baked on a hot plate at 65 C for 2 minutes, then at 95 C for 5 minutes.

4.) The wafers are exposed to UV light (365 nm) under a printed transparency mask for 25 seconds.

5.) Post exposure, the wafers are baked on a hot plate for 2 minutes at 65 C and again for 2 minutes at 95 C.

6.) The photoresist is developed using 1-Methoxy-2-propanol acetate for 1 minute via agitation in a Petri dish or spraying. Afterwards, the remaining developer is washed off with isopropanol and the wafers are blow dried with nitrogen.

7.) The crosslinked photoresist is hard baked on a hot plate at 180 C for 30 minutes. This is an important step, as it additionally hardens the photoresist, so that the wafers can be reused up to 50 times with the pattern remaining intact.

"20 nl PhaseChip" storage layer:

To achieve a 50 um channel height, we use the above recipe, but with the following modifications.

2.) Wafers are coated with photoresist at 1700 rpm for 30 seconds.

3.) The soft bake at 95 C lasts 7 minutes.

5.) The post exposure bake at 95 C lasts 7 minutes.

6.) The developing step lasts 2 minutes.

"65 pl emulsion PhaseChip" storage layer:

This storage layer consists of structures of two different heights. The main flow channel is 50 um high, while the wells are 80 um high.

The channel structure is patterned first and created as described in the "20nl PhaseChip" section (steps 1-5).

6.) After this first patterning step, instead of developing the wafer, however, we coat the wafer again with a new layer of photoresist, as described in the "reservoir layer" section above (steps 2-7) to achieve a 30 um thickness of this second photoresist layer. This ensures that the storage wells are 30 um taller than the main flow channel.

PDMS Fabrication:

STORAGE LAYER	1.) We use Sylgard 184, the ratio of base to curing agent is 10:1, as suggested by the manufacturer. Use 25 g total per device. 2.) Mix and degas for 6 minutes. 3.) Line a round Petri dish with aluminum foil, place a patterned silicon master with the storage layer imprinted on it (see Master Fabrication Protocol). Pour mixed PDMS on the wafer, desiccate for 15 minutes or until air bubbles stop rising from the PDMS, then bake it in oven at 65 C for 60 minutes (+- 5 minutes). Let PDMS cool down at room temperature for 5-10 minutes, then cut out PDMS with a scalpel and peel it off of the wafer**.** 4.) Punch holes from design side (needle gauge 27 for PTFE tubing of 500 um outer diameter). 5.) Clean design side with laboratory tape, not with solvents.

RESERVOIR LAYER	6.) Vapor deposit Chlorotrimethylsilane for least 15 min on the surface of the reservoir master. 7.) Prepare a 10:1 mixture of Sylgard 184 as described above. A total of 3 g of base and curing agent per device is needed. It is important to use fresh PDMS (no more than 15 minutes old). The older and more viscous the PDMS, the thicker the PDMS membrane. The viscosity doubles within the first hour after mixing. 8.) Spincoat PDMS on the reservoir master: the first spin stage is at 800 rpm (5 seconds long); the second spin stage is at 1100 rpm (30 seconds long). The membrane thickness largely depends on a) the height of resist and b) the complexity of the design. For the PhaseChip reservoir, the resulting membrane thickness is on average 30 um. . 9.) Wait two minutes before placing spin-coated wafers on the hot plate. Then bake them at 85 C for 15 min.

BOND LAYERS (PDMS TO PDMS)	10.)Place a) reservoir wafer with spin-coated PDMS layer on it and b) peeled off storage PDMS layer in different places in the plasma chamber, so that they do not touch. Plasma protocol: create vacuum (200 mTorr, +-50 mTorr), then introduce oxygen until the pressure inside the plasma chamber is 500 mTorr (+- 50 mTorr). Turn on power (60W) for 8 seconds (+- 2 seconds). Take out the two pieces, align them (exact alignment does not matter in these designs) and place the storage layer on top of the reservoir layer. The two layers automatically stick to each other without air bubbles forming between them. Bake the assembled device in the oven for at least 30 minutes (but no more than 24 hours) at 65 C. Heating up the device this way reinforces the plasma bond.
BOND PDMS TO SUBSTRATE	11.)Cut with scalpel around the edge of the thick PDMS slab on the assembled device wafer, so that the scalpel penetrates the thin PDMS membrane. Slowly and gently peel off both layers off the reservoir master. Avoiding mistakes during this step is crucial, as any tears in the membrane during the peeling off make the device unusable. 12.)Punch holes into the thin PDMS layer from the design side like explained above. Note that these holes are now going through both PDMS layers. 13.)Bond the assembled device to an untreated silicon wafer using the plasma machine (like in step 10.). Then bake overnight in the oven at 65 C.

SURFACE TREATMENT	14.)If the device is to be used for protein studies, pretreat it with Cytop. Cytop is a fluorinated compound that coats the PDMS channels and prevents protein from sticking to the channel walls. The Cytop treatment works best, if the device is at least one day old. This is because the plasma treatment renders PDMS hydrophilic, and it takes up to 24 hours for the PDMS to relax back to its hydrophobic state and better absorb Cytop. Use CTL 809 Cytop, concentration 0.25%, (Bellex International). Fill the flow layer completely with Cytop (a 50 ul/hr flow rate is appropriate). Do not flush it out. Bake the device at 200 C for 2 hours on a hot plate. At this temperature, the solvent evaporates and Cytop glassifies, coating the PDMS channel walls. Let the device cool down to room temperature and wait 24 hours before use.

Contrary to our previous fabrication protocol[51], where we used base and curing agent in the ratios of 5:1 for the storage layer and 20:1 for the reservoir layer, we now use PDMS in the recommended ratio of 10:1 for both device layers. As a result, the thin membrane that separates the drop storage layer from the reservoir is stronger and does not tear easily, thereby increasing the number of fully functioning device. Another improvement we introduced is using oxygen plasma for bonding two PDMS layers together, rather than heat-induced crosslinking across the two surfaces. As a consequence, the chemical bond between the layers is very strong, eliminating previous problems such as gas bubbles forming at the interface. This modification in the fabrication protocol, too, greatly increases the yield of functioning devices.

Chapter 8: Studying Quench Time and Volume Dependent Crystal Nucleation in Lysozyme Using Microfluidics

Šeila Selimović and Seth Fraden

(Reproduced with permission from *Crystal Growth & Design*, submitted for publication.

Abstract

We employ a new version of the PhaseChip, our microfluidic crystallization platform, for statistical studies of crystal nucleation in Lysozyme in the presence of sodium chloride. The PhaseChip is a (poly)dimethylsiloxane (PDMS) device that allows us study up to 1600 independent nanoliter sized drops simultaneously by controlling their concentration and temperature both spatially (across the chip) and temporally. By choosing an appropriate temporal profile of the temperature we can first increase and then decrease the supersaturation of the protein solution and so decouple crystal nucleation from growth. In each experiment we vary the drop volume (4nl and 20 nl) and nucleation time and count the resulting number of crystals per drop to determine the nucleation rate as a function of drop volume. We also measure the induction time and compare our results to the theoretical prediction.

Introduction

In this paper, we apply the PhaseChip, our microfluidic protein crystallization platform, to determine the nucleation rate of Lysozyme in the presence of sodium chloride as a function of drop volume and nucleation time. The PhaseChip is a two-layer microfluidic devices made of (poly)dimethylsiloxane. Aqueous droplets are stored in the flow layer of the device. The two versions of the PhaseChip employed here house either 800 20 nl drops (this is the "20 nl PhaseChip") or 1600 4 nl drops (this is the "4 nl PhaseChip") in individual wells in the flow layer and have been described in detail elsewhere[68]. Less than 2 μl of solution are needed to fill all wells in either device, and the drops are formed via the "store, then create" method[69]. A key advantage of this drop formation and storage method is that it does not require complex microfluidic elements such as peristaltic valves or nozzles and that there is no start-up time during which precious protein could be lost. Furthermore, all droplets are identical and isolated from each other with fluorinated oil, thus they can be regarded as hundreds of independent experiments.

Underneath and separated from the flow layer by a 30 μm thin PDMS membrane is the reservoir layer with twelve channels that carry sodium chloride solutions. The membrane is permeable to water, but not to salt or protein. When the solution inside a reservoir channel and the solution inside a droplet directly above it differ in solute concentration, then water can permeate through the membrane from the reservoir channel into the droplet or in the opposite direction, thereby changing the concentration of all solutes inside the drop[70]. By choosing the appropriate salt concentration in the reservoir we can use this mechanism to keep the concentration of solutes in all droplets on the PhaseChip steady for the duration of the experiment. Since there is a leakage flux of water from the drops to the outside, the drops never equilibrate with the reservoir. Rather,

they reach a steady state, in which the concentrations of the drop and reservoir vary by 0.3 M.[70] Both PhaseChip versions, the 4 nl PhaseChip and the 20 nl PhaseChip, utilize the same reservoir design.

Last, the PhaseChip is placed on a thermal stage, in which two independent thermoelectric coolers (TEC) are positioned at the ends of a 1 mm thin brass plate. The two TECs can be set to either different temperatures in the range from 2 °C to 40 °C, generating a spatial temperature gradient across the PhaseChip. Alternatively, they can be set to the same temperature.[68] A LabView software allows us to program the temporal profile of the temperature on either TEC. In one experiment, for example, we may choose to store several hundred identical droplets on the PhaseChip and then apply a spatial temperature gradient across the chip. In another experiment, we may apply no spatial gradient, but impose the same time-variable temperature profile on both TECs, such that all drops on the PhaseChip experience the same temperature at any given moment.

A key attribute of the PhaseChip is that it allows hundreds of crystallization trials to be conducted simultaneously, which improves the statistical validity of our results. Previously, we have shown how the solute concentrations can be reversibly varied by adjusting the concentration of the reservoir solution.[71] This allows for multiple cycles of supersaturation per sample within a closed device and for decoupling crystal nucleation from growth. A drawback of this experimental procedure is that the supersaturation of protein varies during the nucleation period, making it difficult to calculate the nucleation rate. There are other microfluidic systems that enable changes in concentration and thus in supersaturation of the protein inside the droplets, such as free interface diffusion (Hansen et al.[72]) or vapor diffusion experiments (Gerdts et al.[73]), but these changes are not reversible. Another way to achieve reversible supersaturation changes in protein

droplets is by utilizing temperature quenches (Galkin and Vekilov[74]), which is the approach we take in this paper. With this method we can decouple nucleation and growth mechanisms while keeping the protein supersaturation steady during either step and vary the nucleation time in order to study the nucleation rate.

We base our analysis of the nucleation rate of Lysozyme on the classical nucleation theory[75], and its application in the work of Galkin and Vekilov[76] and Fichthorn and Weinberg[77]. Our results confirm the theoretical prediction that the nucleation rate scales linearly with drop volume and nucleation time, as long as the amount of protein bound in the crystal nuclei is much smaller than the amount of protein available in the solution.

Experiment

Materials

The protein solution is first prepared off-chip and contains 80 mg/ml Lysozyme (Sigma, product number L-7651), 0.1 M NaAc (Fisher) at pH 4.8. The precipitant solution is prepared and filtered off-chip (0.2 μm syringe filter, Corning, product number 431212) and contains 0.1 M NaAc at pH 4.8 and 1 M NaCl (6% w/v, Fisher). Then, the two solutions are mixed in a 1:1 ratio, so that the resulting protein concentration becomes 40 mg/ml and the concentration of salt is 0.5 M. Because the protein concentration in the stock solution is relatively high, we sometimes observe small crystals in the solution after 24 hours, making our experimental results difficult to reproduce. To avoid this source of error, we prepare a fresh protein solution at most one hour before each experiment.

The protein solution is injected into the device via polytetrafluoroethylene (PTFE) tubing (300 μm inner diameter, Cole Parmer), and the carrier fluid is fluorocarbon oil

(Perfluoro compound FC43, Acros) with surfactant (12% w/w 1H,1H,2H,2H-Perfluoro-1-octanol, Fluka). After the drops are formed via the "store, then create" method[69] at 50 µl/hr, the oil keeps flowing at 5 µl/hr to flush out any remaining impurities from the flow layer. The surfactant lowers the surface tension and so facilitates the drop formation. More importantly, it prevents the protein from coating the channel walls. This measure is in addition to and has the same purpose as coating the PDMS walls before the experiment with CYTOP 809 (Bellex International), a fluorinated compound, at 0.25% v/v concentration.

The PhaseChip is imaged using an automated 3-axis microscope stage with a 4x objective lens and a resolution of 10 µm. We record images of the aqueous drops every 20 minutes, which allows us to chronicle the time and temperature at which crystals first become visible and to count the number of crystals formed in each drop.

Experimental procedure

In this study we conduct two different types of experiment. Type 1 is an exploratory experiment that serves to determine the protein concentration and temperature range to be used for nucleation studies. We load the 20 nl PhaseChip with 40 mg/ml Lysozyme solution in 0.5 M sodium chloride (NaCl) and 0.1 M sodium acetate (NaAc) at pH 4.8, at room temperature (21°C). We choose a reservoir solution (0.2 M NaCl) that ensures that the concentration of all drops remains constant throughout the experiment and only apply a spatial temperature gradient between 4 °C and 23 °C. After 1 hour we measure the lowest temperature at which no crystals are detected using a thermocouple (model HH21, Omega). This is the desired crystal nucleation or quench

temperature. After a total of 24 hours we measure again the lowest temperature at which we cannot observe any crystals. This is the desired crystal growth temperature.

In Type 2 experiments we use both versions of the PhaseChip, the 4 nl and the 20 nl PhaseChip. We always use the same protein formulation to form droplets at room temperature (21 °C), and in each experiment we keep their concentration constant. Then we apply a temperature gradient as outlined in Figure 1. To achieve a high nucleation rate, we increase the protein supersaturation by lowering the temperature across the whole PhaseChip. This nucleation or quench step occurs at 18 °C, as determined in the Type 1 experiment. After a nucleation or quench time t_n we lower the protein supersaturation by raising the temperature back to room temperature. This step suppresses further crystal nucleation, so that all remaining protein in the aqueous solution is available for crystal growth. Thus, we refer to the first step in this temperature profile as the crystal nucleation step, and the time between t_n and 24 hours (the maximum duration of the experiment) is the crystal growth step. At the end of the experiment we count the number of crystals per drop. We vary two parameters in the experiments of this type: the drop volume (4 nl or 20 nl) by choosing the appropriate PhaseChip version and the quench time t_n (0 to 24 h).

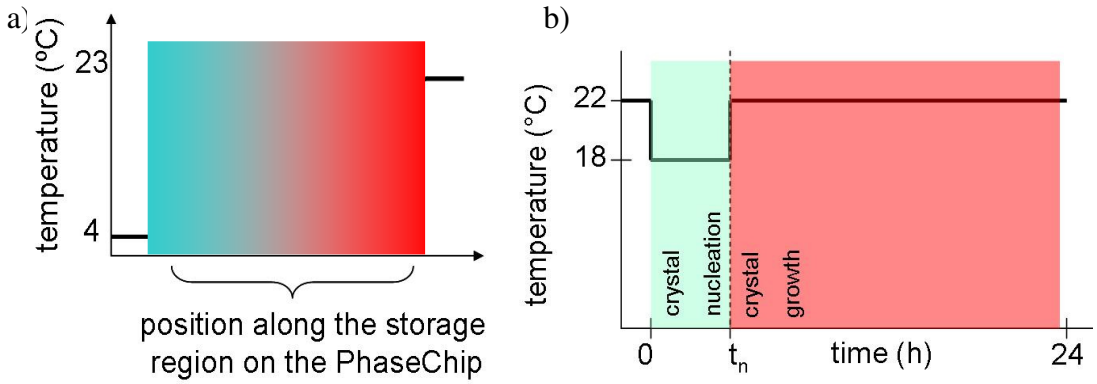

Figure 1. a) Temperature profile in experiment of type I (linear gradient in temperature). b) Typical temperature profile for crystal nucleation experiments (type II). The protein solution is loaded and drops are formed at 21 °C, after which the temperature is reduced to 18 °C. After a nucleation or quench time t_n, the temperature is raised back to 21 °C to optimize crystal growth. The experiment ends after a total of 24 hours.

Results and discussion

In the exploratory experiment (Type 1) we determine the nucleation and growth temperature suitable for our experimental setup. There are two major constraints to be considered:

a) We conduct many nucleation experiments in this study, so each experiment should last no longer than 24 hours, and week-long experiments like those described before[71] are not convenient for this study. One way to achieve that is to use a high-concentration protein solution (40mg/ml), which is supersaturated (solubility is C_s = 1.56 mg/ml at room temperature, and supersaturation S = 26.6[78]) already at the beginning of the experiment. This means that crystal nuclei form very quickly, ideally on the order of an hour. If stable nuclei were formed faster than that limit, however, then our imaging system could not provide data with sufficient time resolution, as data is collected every twenty minutes. Hence, these two numbers, 1 hour and 24 hour, provide the time frame for our experiments, so we can determine the nucleation and growth temperatures.

b) The PhaseChip is open to the environment and not humidity controlled. If we choose a nucleation temperature that is too low (generally below 10 °C in our laboratory), after a few minutes beads of water start collecting on the surface of the PhaseChip,

impacting the quality of the recorded images and the temperature distribution inside the microfluidic device. Thus, the desired nucleation temperature should be in the range between 10 °C and room temperature for a 40 mg/ml Lysozyme solution.

Figure 2 displays a stitched image of the PhaseChip with 800 20 nl wells. All drops have the same concentration during the experiment, and the temperature increases from 4°C to 23°C (from left to right in the image). After one hour, crystals can be detected at 18 °C and below (examples are shown in Figure 2), indicating that this is the appropriate nucleation temperature for future experiments. After 24 hours, crystals are detected at temperatures up to 23 °C. Literature data[79] suggests that at above 23 °C and the pH and salt conditions used here the orthorhombic Lysozyme crystal structure has a lower solubility than the tetragonal morphology. In order to simplify our results, we confine our experiments to a region where the tetragonal Lysozyme structure is favored, and thus choose a lower temperature, 21 °C, as the crystal growth temperature.

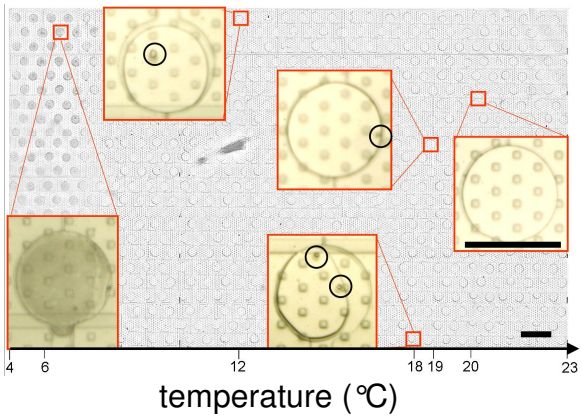

Figure 2. Stitched image of the 20 nl PhaseChip used in the exploratory experiment. The temperature increases from left (4 °C) to right (23 °C). Red squares and framed high-magnification images identify typical drops at a particular temperature. The drop at 20 °C contains no detectable crystals, while the drops below 18 °C do (crystals are circled in

black). The left most image, at 6 °C, shows a drop containing a gel phase, rather than a macroscopic crystal. The large scale bar is 600 μm, the small scale bar is 2 mm.

Reproducibility

In the nucleation experiments (Type 2) we first assess the reproducibility of our tests. We accomplish this by conducting two 30 min quench experiments at 18 °C in two separate 20nl PhaseChip devices. At the end of the experiments we count the number of crystals per drop and plot this distribution in Figure 3. We prepare a fresh Lysozyme solution for each experiment, and we fabricate two PhaseChips on the same day, in order to eliminate variation due to PDMS container lot. Other sources of variation remain, however: Because we fabricate the two devices at the same time, we use two different silicon masters, and the imprinted channels on these masters can vary up to 5 μm in height (the average height on all masters is 50 μm). This variation in height means that the well volume and therefore the volume of stored drops can vary by up to 2 nl, which affects the nucleation rate. Further, the two experiments were conducted at different days. Even though the temperature on-chip was well-controlled, it is possible that the change in ambient humidity and temperature had an effect on the nucleation rate. The two crystal distribution curves match to within 15% of each other, and the experimentally extracted values of N_{mean} (average number of crystals per drop) in the two experiments are 0.69 and 0.93 (blue and red curves, respectively). In addition, we use N_{mean} to calculate the Poisson Law distribution

$$P(m) = \frac{N_{mean}^{\ m}}{m!} e^{-N_{mean}} \tag{8.1}$$

where m is the number of crystals per drop. The corresponding Poisson predictions for the normalized number of drops are also shown in Figure 3. Considering the variability in the microfluidic chips and the effect environmental factors (humidity and ambient temperature) potentially have on the nucleation rates, we find that our experiment is reproducible to within 15% of each data point in the crystal number distribution, and that the distributions have a strong Poisson behavior.

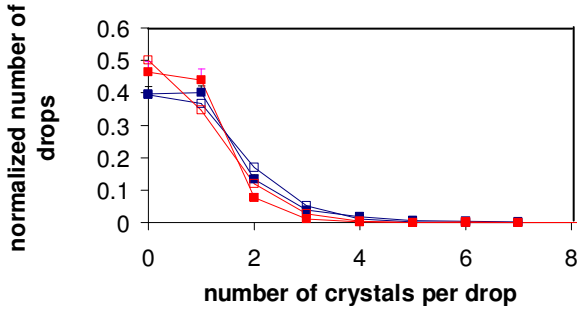

Figure 3. Distribution of nucleated crystals per drop in two 30-minute quench experiments (red and blue filled squares). Error bars are included. Empty red and blue squares denote the corresponding Poisson prediction, calculated by using the experimental value for the average number of crystals per drop (N_{mean}).

Nucleation rate measurements

Since we have established that our nucleation results are reproducible, we now conduct a series of quench experiments on both 4 nl and 20 nl drops. Even though each device can hold up to 800 or 1600 droplets, depending on size, not all wells are always filled with drops, and sometimes the two PDMS layers (flow and reservoir layer) are improperly aligned, so that not all drops are concentration controlled through the

reservoir. There are, however, always at least 450 concentration controlled drops in each device and in every experiment reported here. In addition to the previously described quench experiments we also conduct an experiment with a 24 hour long quench, that is the temperature remains at 18 °C throughout the experiment and there is no separate growth period. The goal here is to measure the maximum N_{mean} possible for the given Lysozyme solution and drop size. In addition, a final experiment is conducted at 22 °C for 24 hours on each PhaseChip version and has no separate nucleation period; in this case the nucleation period is 0 h long. Our aim in this experiment is to establish the N_{mean} due to the already supersaturated protein solution. All measured distributions of the number of nucleated crystals per drop display Poisson behavior, as evident from the comparison with the predicted Poisson Law distribution (Figure 4).

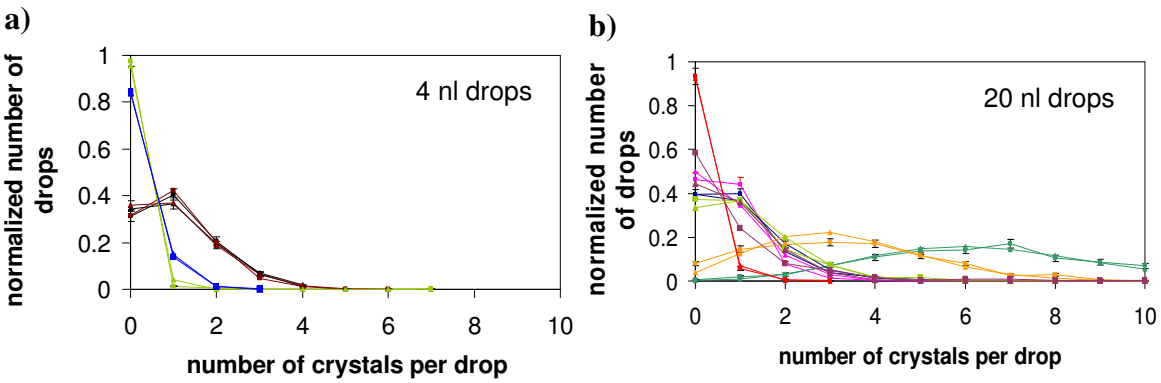

Figure 4. Crystal distribution curves and Poisson Law predictions for (a) 4 nl drops and (b) 20 nl drops. (a) 0 hr quench (—), 0.17 hr quench (—), 1.75 hr quench (—), 24 hr quench (—). (b) 0 hr quench (—), 0.25 hr quench (—), 0.5 hr quench (—), 0.75 hr quench (—), 1 hr quench (—),24 hr quench (—). Filled squares denote the experimental data, filled triangles denote the Poisson Law prediction. (Online in color.)

Table 1 contains a list of quench times t_n and the corresponding values of N_{mean} for each drop size. Because variations in silicon masters and thus in PhaseChip channel dimensions have shown to introduce systematic error in our nucleation measurements, we now only use devices stemming from the same sets of masters and thus in Table 1 report the N_{mean} value for t_n =0.5 h for 20 nl drops as 0.93, rather than the average of two measurements reported above. We also note that after a quench time of 1 hour first crystals become visible. At longer nucleation times, particularly beyond t_n = 2 h we cannot guarantee that nucleation and growth are fully decoupled and therefore do not conduct further experiments.

Table 1. Average number of crystals per drop (N_{mean}) as a function of quench time t_n for 4 nl and 20 nl size drops.

4 nl	t_n **(h)**	0	0.17	1.75	24
drops	N_{mean}	0.04	0.18	1.02	1.50

20 nl	t_n **(h)**	0	0.25	0.5	0.75	1	24
drops	N_{mean}	0.08	0.81	0.93	1.01	3.27	7.02

The data shown in Table 1 is plotted in Figure 5 (filled icons). The nucleation rate J [#crystals /cm^{3}s] is described as

$$J = AC(t)e^{-\frac{B}{\sigma(t)^2}} \qquad (8.2)$$

where $t = t_n$, V is the drop volume, $C(t) = C$ [mg/ml] is the protein concentration, A and B are expression constants. The constant A is a measure of the nucleation kinetics and the

constant B is related to the surface tension of the crystal in solution and depends on the temperature. The quantity σ is the protein supersaturation and is defined as

$$\sigma = \ln\left(\frac{C}{C_s}\right), \tag{8.3}$$

where C_s [mg/ml] is the protein solubility. The number of crystals per drop N can be fit to the following expression:

$$N = \int_0^{\infty} V(t)\, A\, C(t)\, e^{\frac{-B}{\sigma(t)^2}}\, dt\,, \tag{8.4}$$

where $t = t_n$, V is the drop volume, C is the protein concentration, A and B are expression constants, and σ is the protein supersaturation. In our experiments these parameters do not vary with time, except for the supersaturation, because it changes with temperature, but the supersaturation is, too, constant during the nucleation period. The expression for the homogeneous nucleation rate then simplifies to

$$J = N/Vt. \tag{8.5}$$

The measured nucleation rate J indeed initially proves to be constant in time (t_n), and when the solution becomes depleted, it develops a time-dependence. Further, it is independent of volume V: for 4 nl drops the nucleation rate is 34.72 crystals/cm^{3}s, and for the five times bigger drops of 20 nl it is similar, namely 38.19 crystals/cm^{3}s.

As mentioned previously, we conduct a 24 hour quench experiment on both drop sizes to determine the maximum possible number of crystals per drop. We count the crystals at the end of that experiment (at 24 hours), but we also count the crystals two and sixteen hours into the experiment, that is, at a time when both nucleation and crystal growth are ongoing and are not decoupled from each other. The purpose of these measurements is to establish the time at which the solution becomes depleted of protein

monomers, i.e. the concentration of protein in the solution changes noticeably. We fit a straight line to this data extracted from the 24 hour quenches for both droplet sizes and note that the slopes of these curves are much smaller than at the beginning of the experiment, namely 0.90 crystals/cm^{3}s and 1.80 crystals/cm^{3}s for the 4 nl and 20 nl drops, respectively, indicating that nucleation is now suppressed. We also posit that the intersection of the two linear fit curves gives us the time at which the protein solution becomes depleted and the amount of protein available in solution is much smaller than originally assumed.

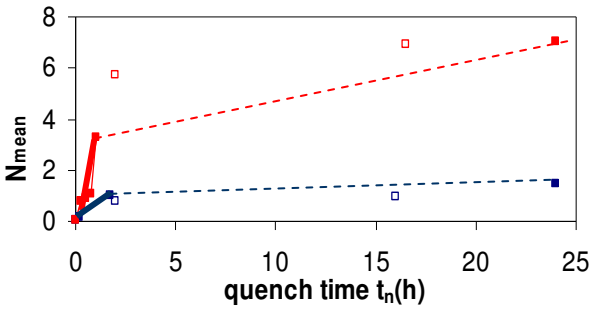

Figure 5. Average number of crystals per drop (N_{mean}) as a function of quench time for 4 nl drops (blue filled squares) and 20 nl drops (red filled squares). The full red and blue lines are linear fits to the data for quench times 0 to 1hr and 0 to 1.75 hr (for 20 nl and 4 nl drops, respectively), when crystal nucleation and growth are decoupled. The blue and red empty squares are data extracted from the 24 hour quench experiments and the blue and red dashed lines are the corresponding linear fits. (Online in color.)

Induction time measurement

Induction time is defined as the time it takes a crystal to grow from a nucleus to a detectable size. This size depends on the resolution of the imaging system and is 10 μm in

our case. Following the treatment in Bowerman et al.[80] and Ahrens et al.[81] we calculate the cumulative distribution function (CDF) for a Poisson distribution and a time-independent nucleation rate *J*:

$$CDF = 1 - e^{-JVt_n} . \qquad (8.6)$$

This equation describes the probability of detecting at least one crystal per drop at a time *t*. The time at which the function reaches 1-1/e of its maximum value is interpreted to be the induction time. Then, the predicted induction time for 4 nl (with J = 34.72 crystals/cm^{3}s) and 20 nl drops (with J = 38.19 crystals/cm^{3}s) is 2 hours and 0.3 hours, respectively (Figure 6). The theory, however, assumes that the growth time is negligible compared to the time it takes to form a stable nucleus. We therefore expect our experimental value for induction time to be the same as the predicted value, if not larger.

We measure the experimental value of the induction time by counting the number of drops with at least one crystal at different intervals of the 24 hour quench experiment. The resulting curve has a sigmoidal shape, and the point of inflection is understood to occur at a time that equals the induction time. For 4 nl drops, this occurs at 3 hours, rather than the predicted 2 hours, and for 20 nl drops, it occurs earlier, namely at 1.2 hours, instead of the predicted 0.3 hours. This discrepancy is likely due to the fact that the crystal growth time is finite and cannot be neglected, as assumed in the theory, although we did not measure the growth rate. It is also expected that the induction time is shorter for larger volume drops, as the nucleation rate there is higher. The CDF curves, as well as the experimental measurement of the number of drops with at least one crystal are plotted as a function of quench time in Figure 6.

There is a noticeable difference between the predicted PDF and the experimental values for the 4nl droplets. The experimental curve approaches a value close to 0.6, rather than

1, which is not in accordance with the theory. We suspect that there is a different mechanism at play in the 4nl case than in 20 nl drops, or the same discrepancy should occur in both sets of data. It is possible that in the 24 hour quench for the 4nl drops either the protein solution was not homogeneous (i.e. was not mixed well prior to drop formation), so that different drops in fact have different concentrations of protein and salt. Further, this discrepancy can be explained by an anomaly in the temperature profile. If the temperature had risen for a certain amount of time above 18 °C (even just to 19 °C) on one side of the chip, this would have impacted the nucleation behavior in the affected drops. Last, if there are two nucleation mechanisms involved, e.g. homogeneous and heterogeneous nucleation, and heterogeneous nucleation (which is not described in the theoretical treatment used here) had a much higher nucleation rate, then that could explain the discrepancy between the experimental results and the theoretical prediction.

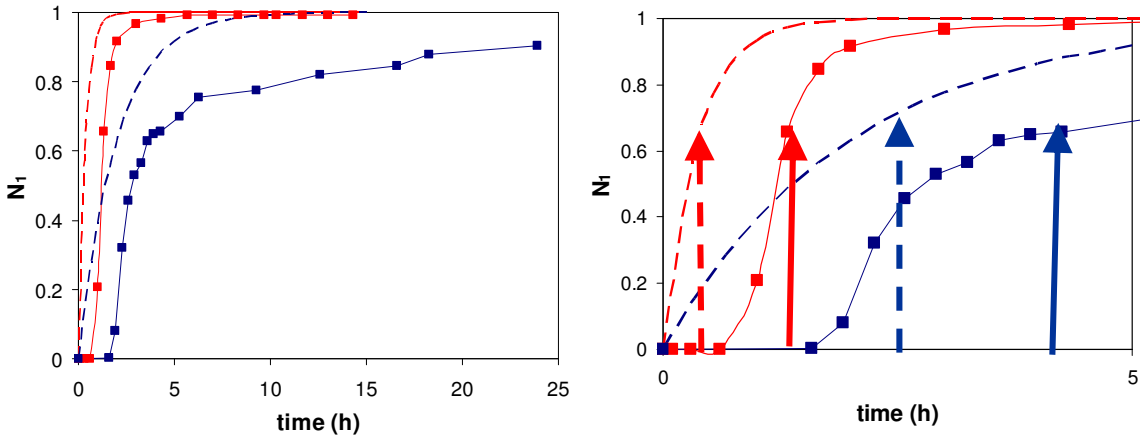

Figure 6. Number of drops with at least one crystal (N_1) as a function of time (left image: 24 hour span, right image: view of the first five hours). Red denotes 20 nl drops, blue denotes 4 nl drops. The thin dashed curves denote the cumulative distribution functions, and the connected red and blue squares are the experimental data for the two drop sizes. The thick dashed and continuous lines in red and blue indicate the projected and the

experimental induction time values for 20 nl and 4 nl drops, respectively. (Online in color.)

Conclusion

We have shown that the PhaseChip is a promising device for protein crystallization, in particular for statistical studies of crystal nucleation. Varying the temperature of protein drops on-chip is a practical way to control protein supersaturation levels, and varying the quench time and drop volume allows us to study the nucleation rate of protein.

The 0 hour quench experiment indicates that even though we begin our experiments with a highly supersaturated solution (S = 26.6), the average number of crystals per drop nucleated in a 24 hour period is less than 0.1. Therefore, we can assume that no or very few crystals nucleate during the growth period at 21 °C and crystal nucleation is fully decoupled from growth. Next, our experimental results agree with the expectation that the nucleation rate scales linearly both with quench time and with the drop volume, as long as the protein solution is not depleted. The measured nucleation rates are J = 34.72 crystals/cm^{3}s for 4 nl drops and J = 38.19 crystals/cm^{3}s 0.5 for 20 nl drops. Our analysis suggests that the solution is significantly depleted after a nucleation period of 2 hours for both drop sizes, suggesting that at quench times shorter than 2 hours the nucleation rate is time-independent and can be described with the classical nucleation theory. At quench times longer than 2 hours, however, the nucleation rate becomes time-dependent.

From these experiments we also extract information about the induction time of the Lysozyme crystals. Calculation of the probability distribution function of the Poisson

distribution indicates that the induction times for the 4 nl and 20 nl drops should be 2 hours and 0.3 hours, respectively, for the case where the crystal growth time is negligible. We posit, however, without having measured the growth rate, that in reality this time cannot be neglected, especially since our imaging system detects crystals only at a relatively large size of 10 μm. In our 24 hour nucleation experiments we measure 3 hours and 1.2 hours for the 4nl and 20 nl induction times, which is in compliance with the predicted results.

Future experiments will focus on nucleation rate measurements in a variety of drop sizes to show whether the nucleation rate always scales linearly with drop volume or if there is a minimum drop volume at which this relationship fails. We will also conduct experiments at different quench temperatures to study the effect of protein supersaturation on the nucleation rate. These measurements will yield more nucleation rate values that we can then compare with literature data to see whether there are large discrepancies between the microfluidics and standard approaches to nucleation rate measurements.

Chapter 9. Outlook

There are several new avenues we can envision for the use of the PhaseChip. For example, incorporating fluorescence imaging into the experimental setup, so we can record both brightfield and fluorescence images of protein solutions, would be helpful in detecting protein crystals and distinguishing them from salt crystals. Further, there are currently plans for combining DLS (dynamic light scattering) with our microfluidic setup. That would allow us to detect protein crystals at a very early age (nuclei of only several protein molecules rather than 10 μm large macrocrystals). This information, in turn, would be used to adjust the experimental condition (concentration or temperature) at the right time in order to decouple crystal nucleation and crystal growth more efficiently. Another improvement that could be made is making membranes between the storage layer and the reservoir from a material other than PDMS. Cellulose membrane, for example, could be used to control the pH levels of the protein solution, as small molecules can pass through such a membrane, but proteins cannot. Currently, when the concentration of solutes (ions, protein) inside a protein solution changes, so does the pH, albeit not to a large degree. Incorporating a cellulose membrane would allow us to explore the pH dependence on the crystal nucleation rates or to explore phase diagrams of polymer in the pH - space. Last and most importantly, combining our microfluidic setup with an x-ray crystallography apparatus would circumvent the problem of crystal

extraction and preservation before x-ray analysis. It has been shown that protein crystals inside PDMS chips can be subjected to x-rays and that the resulting data is comparable to crystallography data collected on crystals outside of PDMS.

Appendix

Appendix I - Master Fabrication Protocol

(Applicable to all versions of the PhaseChip)

Reservoir layer containing no valves:

1.) 3" silicon wafers (Silicon Sense, Inc.) are used as is, without any pretreament.

2.) Wafers are coated with 1 -2 ml of SU8-2025 photoresist. The spin rate is first increased from 0 to 500 rpm, where it remains for 5 seconds. In this step the resist is spread on the whole wafer. Then spin rate is increased to 2800 rpm for 30 seconds to achieve a resist thickness of 30 μm.

3.) The wafers are soft baked on a hot plate at 65 C for 2 minutes, then at 95 C for 5 minutes.

4.) The wafers are exposed to UV light (365 nm) under a printed transparency mask (CASArt Imaging) for 25 seconds.

5.) Post exposure, the wafers are baked on a hot plate for 2 minutes at 65 C and again for 2 minutes at 95 C.

6.) The photoresist is developed using 1-Methoxy-2-propanol acetate for 1 minute. Afterwards, the remaining developer is washed off with isopropanol and the wafers are blow dried.

7.) The resist is hard baked on a hot plate at 180 C for 30 minutes.

This recipe is used for both the reservoir layer containing valves (Selimovic, Jia, Fraden, *CGD* 2009) and the new PhaseChip gradient reservoir (Selimovic, Gobeaux, Fraden, *submitted to Lab Chip* 2009; Selimovic, Fraden, *submitted to CGD* 2009).

Reservoir layer containing valves:

Channels requiring a rectangular cross-section are fabricated in negative photoresist SU8-2025 as described above. Channels that are to serve as valves or pumps are fabricated in positive photoresist as follows:

8.) The wafer is spin coated with Hexamethyldisilanaze, the spin rate is irrelevant, as long the whole wafer is coated.

9.) To achieve a 15 μm thick layer of photoresist, we pour 1-2 ml of positive photoresist SPR 2207 on the wafer, then spin it at 500 rpm for 5 seconds, and then further at 900 rpm for 60 seconds.

10.) The wafer is soft baked at 65 C for 2 minutes, 115 C for 4 minutes, and again at 65 C for 2 minutes.

11.) The wafer is exposed to UV light (365 nm) for 45 seconds.

12.) The photoresist is developed with AZ 400K, which should be first diluted with water in the ratio of 1:4. The developing step (agitation in a Petri dish) lasts on average 1 minute.

13.) The hard-bake (during which the photoresist reflows, thereby changing the channel cross-section from rectangular to a semi-circle) begins at 65C on a hot plate.

Then the temperature is ramped to 200C and kept at that final temperature for 1.5 hours, before the temperature is reduced again to room temperature.

"4 nl PhaseChip" and "20 nl PhaseChip" storage layer:

To achieve a 50 um channel height, we use the above recipe (reservoir without valves), but with the following modifications.

2.) Wafers are coated with photoresist at 1700 rpm for 30 seconds.

3.) The soft bake at 95 C lasts 7 minutes.

5.) The post exposure bake at 95 C lasts 7 minutes.

6.) The developing step lasts 2 minutes.

"65 pl emulsion PhaseChip" storage layer:

This storage layer consists of structures of two different heights. The main flow channel is 50 um high, while the wells are 80 um high.

The channel structure is created as described above (steps 1-5).

6.) Instead of developing the wafer, however, we coat the wafer again with a new layer of photoresist, as described in the "reservoir layer" section above (steps 2-7). This ensures that the storage wells are 30 um taller than the main flow channel.

Appendix II - PDMS Device Fabrication Protocol

STORAGE LAYER	1.) Sylgard 184 base to curing agent ratio = 10:1, as suggested by the manufacturer. Use 25 g total per device. 2.) Mix and degas for 6 minutes (Thinky Mixer). 3.) Line a round Petri dish with aluminum foil, place silicon master with channels imprinted on it in photoresist. Pour mixed PDMS on the wafer, desiccate for 15 minutes, then bake in oven at 65 C for 60 minutes. It does not matter, if the PDMS is overbaked. Let PDMS cool down at room temperature for 5-10 minutes, then cut out PDMS with a scalpel and peel it off of the wafer**.** 4.) Punch holes from design side (needle gauge 27). 5.) Clean design side with laboratory tape.

RESERVOIR LAYER	6.) Vapor deposit Chlorotrimethylsilane for least 15 min on the surface of the reservoir master. 7.) Prepare a 10:1 mixture of Sylgard 184 as described above. A total of 3 g total per device is needed. It is important to use fresh PDMS (no more than 15 minutes old). The older and more viscous the PDMS, the thicker the PDMS membrane. The viscosity doubles within the first 1 hr. 8.) Spincoat PDMS on reservoir master: the first spin stage is at 800 rpm (5 seconds long); the second spin stage is at 1100 rpm (30 seconds long). The membrane thickness largely depends on a) the height of resist and b) the complexity of the design. For all devices introduced in this paper, the resulting membrane thickness is 30 um on average. 9.) Wait two minutes before placing spin-coated wafers on the hot plate. Then soft-bake them at 85 C for 15 min.
BOND LAYERS (PDMS TO PDMS)	10.) Place reservoir wafer with spin-coated PDMS layer on it and storage PDMS layer in different places in the plasma chamber, so that they do not touch. Plasma protocol: create vacuum (200 mTorr), then introduce oxygen until the pressure inside the plasma chamber is 500 mTorr (+- 50 mTorr). Turn on power (60W) for 8 seconds (+- 2 seconds). Take out the two pieces, align them (alignment does not matter in these designs) and place the storage layer on top of the reservoir layer. The two layers will automatically stick to each other without air bubbles forming between them. Bake the assembled device in the oven for at least 30 minutes (but not more than 24 hours) at 65 C.

BOND PDMS TO SUBSTRATE	11.) Cut with scalpel around the edge of the thick PDMS slab on the assembled device wafer, so that the cut penetrates the thin PDMS membrane. Slowly and gently peel off both layers. This step is crucial, as any tears in the membrane during the peeling off make the device unusable. 12.) Punch holes into the thin PDMS layer from the design side like explained above. Note that these holes are now going through both PDMS layers. 13.) Bond the assembled device to an untreated silicon wafer (if the device is to be used on the temperature stage) or to a glass slide using the plasma machine (like in step 10.). Then bake overnight in the oven at 65 C.

SURFACE TREATMENT	14.) If the device is to be used for protein, pretreat it with Cytop. Cytop is a fluorinated compound that coats the PDMS channels and prevents protein from sticking to the channel walls. The Cytop treatment works best, if the device is at least one day old. This is because the plasma treatment renders PDMS hydrophilic, and it takes up to 24 hours for the PDMS to relax back to its hydrophobic state and adsorb Cytop better. Use high boiling temperature Cytop, concentration 0.25%, CTL 809 (Bellex International). Fill the flow layer completely with Cytop (a to 50 ul/hr flow rate is appropriate). Do not flush it out. Bake the device at 200 C for 2 hours on a hot plate. At this temperature, the solvent evaporates and Cytop glassifies, coating the PDMS channel walls. Let the device cool down to room temperature and wait 24 hours to use it.

Bibliography

(1) J.Atencia, D.J.Beebe. "Controlled microfluildic interfaces." *Nature* 437 (2005): 4163.

(2) S. Sia, G.M. Whitesides. "Microfluidic devices fabricated in poly(dimethylsiloxane) for biological studies." *Electrophoresis* 24 (2003): 3563.

(3) J. Shim. "Novel Approach to Protein Crystallization; Control of the Phase Behavior of Aqueous Solutions Using Microfluidics." Dissertation, Brandeis University (2006)

(4) J.Leng, B. Lonetti, P. Tabeling, M. Joanicot, A.Ajdari. "Microevaporators for Kinetic Exploration of Phase Diagrams." *PRL* 96 (2006): 084503.

(5) J.Shim, G.Cristobal, D.R.Link. T.Thorsen, S.Fraden. "Using Microfluidics to Decouple Nucleation and Growth of Protein Crystals." *Crystal Growth & Design* 7 (2007): 2192.

(6) B. Zheng, J.D. Tice, L.S. Roach, R.F. Ismagilov. "A Droplet-Based, Composite PDMS//Glass Capillary Microfluidic System for Evaluating Protein Crystallization Condition by Microbatch and Vapor-Diffusion Methods with On-Chip X-Ray Diffraction." *Angew. Chem. Int. Ed.* 43 (2004): 2508.

(7) B.Zheng, C.J.Gerdts, R.F. Ismagilov. "Using nanoliter plugs in microfluidics to facilitate and understand protein crystallization." *Current Opinion in Structural Biology* 15 (2005): 548.

(8) C.L.Hansen, S.R. Quake. "Microfluidics in structural biology: smaller, faster … better." *Current Opinion in Structural Biology* 13 (2003): 538.

(9) T.Thorsen, T.Maerkl, S.R.Quake. "Microfluidic Large Scale Integration." *Science* 298 (2002): 280.

(10) P. Mitchell. "Microfluidics – downsizing large-scale biology." *Nature biotechnology* 19 (2001): 717.

(11)S.K. Sia, G.M. Whitesides. "Microfluidic devices fabricated in poly(dimethylsiloxane) for biological studies." *Electrophoresis* 24 (2003): 3563.

(12) J.M.Watson, M.G. Barron. "Precise Static And Dynamic Permeation Measurements Using A Continuous-Flow Vacuum Cell." *Journal of Membrane Science* 106 (1995): 259.

(13) G.C.Randall, P.S. Doyle. "Permeation-driven flow in poly(dimethylsiloxane) microfluidic devices." *PNAS* 102 (2005): 10813.

(14) K.Kim, S.Park, H.Manohara, J.Lee. “Polydimethylsiloxane (PDMS) for High Aspect Ratio Three-dimensional MEMS.” *Int. Sym. Mechatronics Intelligent Mech. Sys* (2000):55.

(15) J.C.McDonald, D.C.Duffy, J.R.Anderson, D.T.Chiu, H.Wu, O.J.A.Schueller, G.M.Whitesides. “Fabrication of microfluidic systems in poly(dimethylsiloxane).” *Electrophoresis* 21 (2000): 27.

(16) T. Thorsen, S.J. Maerkl, and S.R. Quake. "Microfluidic large-scale integration," *Science* 298 (2002): 580.

(17) K.T. Kotz, S. Nagrath. “Lab Module 1: PDMS Device Fabrication.” BioMEMS Resource Center. http://www.biomemsrc.org/biomems/documents/Lab_module_1_PDMS.pdf

(18) V. Studer, G. Hang, A. Pandolfi, M. Ortiz, W.F. Anderson, S.R. Quake. “Scaling properties of a low-actuation pressure microfluidic valve.” *J. Appl. Phys.* 95 (2004): 393.

(19)M.A.Unger, H.Chou, T.Thorsen, A.Scherer, S.R. Quake. “Monolithic Microfabricated Valves and Pumps by Multilayer Soft Lithography.” *Science* 288 (2000): 113.

(20) J.Goulpeau, D.Trouchet, A.Ajdari, P.Tabeling. “Experimental study and modeling of polydimethylsiloxane peristaltic micropumps.” *J. Appl. Phys*. 97 (2005): 1.

(21) Th. Ward, M. Faivre, M. Abkarian, H.A.Stone. “Microfluidic flow focusing: Drop size and scaling in pressure *versus* flow-rate-driven pumping.” *Electrophoresis* 26 (2005): 3716.

(22) P.Garstecki, M.J. Fuerstman, H.A. Stone, G.M. Whitesides. “Formation of droplets and bubbles in a microfluidic T-junction – scaling and mechanism of break-up.” *Lab Chip* 6 (2006): 437.

(23) J.U. Shim, G. Cristobal, D.R. Link, T. Thorsen, Y.W. Jia, K. Piattelli, and S. Fraden. "Control and measurement of the phase behavior of aqueous solutions using microfluidics," *JACS* 129 (2007): 8825.

(24) O. Galkin, P.G. Vekilov, *J. Phys. Chem. B* 103 (1999): 10965.

(25) S. Selimovic, Y. Jia, S. Fraden. *Crystal Growth & Design*, 9 (2009): 1806.

(26) J.U. Shim, G. Cristobal, D.R. Link, T. Thorsen, S. Fraden, *Crystal Growth & Design* 7 (2007): 2192.

(27) P.G. Vekilov, O. Galkin, *Colloids and Surfaces A: Physicochem. Eng. Aspects* 215 (2003): 125.

(28) S.B. Howard, P.J. Twigg, J.K. Baird, E.J. Meehan, *Journal of Crystal Growth* 90 (1988): 94.

(29) H.D. Young, *Statistical Treatment of Experimental Data* (New York: McGraw-Hill, 1962).

(30) R.F. Fisher, F. Yates, Eds. *Statistical tables for biological, agricultural, and medical research* (Edinburgh: Oliver and Boyd, 1963).

(31) P.G. Vekilov, L.A. Monaco, B.R. Thomas, V. Stojanoff, F. Rosenberger, *Acta Crystallogr., Sect. D* 52 (1996): 785.

(32) P.G. Debenedetti, *Metastable Liquids. Concepts and Principles.* (Princeton: Princeton University Press, 1996).

(33) D. Kashchiev, *J. Chem. Phys.* 76 (1982): 5098.

(34) D.W. Oxtoby, D. Kashchiev, *J. Chem. Phys.* 100 (1994): 7665.

(35) D.W. Oxtoby, R. Evans, *J. Chem Phys.* 12 (1988): 7521.

(36) S. He, P. Attard. *Phys. Chem. Chem. Phys.* 7 (2005): 2928.

(37) M.P. Moody, P. Attard, *Phys. Rev. Lett*. 91 (2003): 56104.

(38) J.M. Garcia-Ruiz, *Journal of Structural Biology* 142 (2003): 22.

(39) K. Boxshall, M. Wu , Z. Cui, Z. Cui, J. F. Watts, A.M. Baker *Surf. Interface Anal.* 38 (2006): 198.

(40) P. Laval, J.B. Salmon, M.Joanicot, *J. Crystal Growth* 303 (2007): 622.

(41) C.F. Zukoski, A.M. Kulkarni, N.M. Dixit, C*olloids and Surfaces A: Physicochem. Eng.Aspects* 215 (2003): 137.

(42) N.L. Jeon, S.K.W. Dertinger, D.T. Chiu, I.S. Choi, A.D. Stroock, G.M. Whitesides, *Langmuir* 16 (2000): 8311.

(43) L. Li, D. Mustafi, Q. Fu, V. Tereshko, D. Chen, J. Tice, R. Ismagilov, *PNAS* 103 (2006): 19243.

(44) C. Hansen, S. Quake, *Current Opinion in Structural Biology* 13 (2003): 538.

(45) C.J. Gerdts, V.Tereshko, M.K. Yadav, I. Dementieva, F. Collart, A. Joachimiak, R.C. Stevens, P. Kuhn, A. Kossiakoff, and R.F. Ismagilov, *Angew Chem Int Ed Engl*. 45 (2006): 8156 and C.J.Gerdts, M.Eliott, S.Lovell, M.B.Mixon, A.J.Napuli, B.L.Staker, P.Nollert, and L.Stewart, *Acta Cryst. D - Biological Crystallography* 64 (2008): 1116.

(46) C.L. Hansen, E. Skordalakes, J.M. Berger, S.R.Quake, *Proc. Nat'l Acad. Sci.* 99 (2002): 16531.

(47) J. Leng and .J.-B. Salmon, *Lab Chip* 9 (2009): 24.

(48) S.L. Perry, G.W. Roberts, J.D. Tice, R.B. Gennis, and P.J.A. Kenis. *Crystal Growth & Design* 9 (2009): 2566.

(49) K. Dhouib, C.K. Malek, W. Pfleging, B. Gauthier-Manuel, R. Duffait, G. Thuillier, R. Ferrigno, L. Jacquamet, J. Ohana, J.L. Ferrer, A. Theobald-Dietrich, R. Giege, B. Lorber, and C. Sauter. *Lab Chip* 9 (2009): 1412.

(50) Š. Selimović, Y. Jia and S. Fraden, *Crystal Growth & Design* 9 (2009): 1806.

(51) J.U. Shim, G. Cristobal, D.R. Link, T. Thorsen, Y.W. Jia, K. Piattelli, and S. Fraden, *JACS* 129 (2007): 8825.

(52) O. Galkin and P. Vekilov, *J. Phys. Chem. B* 103 (1999): 10965.

(53) J.R. Luft, J.R. Wolfley, M.I. Said, R.M. Nagel, A.M. Lauricella, J.L. Smith, M.H. Thayer, C.K. Veatch, E.H. Snell, M.G. Malkowski, and G.T. DeTitta. *Protein Science* 16 (2007): 715.

(54) N. L. Jeon, S. K. W. Dertinger, D. T. Chiu, I. S. Choi, A. D. Stroock, and G. M. Whitesides, *Langmuir* 16 (2000): 8311.

(55) C. Hansen , S. Quake, *Curr. Opin. Struct. Biol.* 13 (2003): 538.

(56) H. Song, D.L. Chen, and R.F. Ismagilov. *Angewandte Chemie-International Edition* 45 (2006): 7336.

(57) P. Laval, A. Crombez, J.-B. Salmon, *Langmuir* 25 (2009): 1836.

(58) H. Boukellal, S. Selimovic, Y. Jia, G. Cristobal, and S. Fraden, *Lab Chip* 9 (2009): 331.

(59) C. Holtze, A.C. Rowat, J.J. Agresti, J.B. Hutchison, F.E. Angilè, C.H.J. Schmitz, S. Köster, H.D. Katherine J. Humphry, R. A. Scanga, J.S. Johnson, D. Pisignano, D. A. Weitz, *Lab Chip* 8 (2008): 1632.

(60) G.M. Thurston, *PNAS* 104 (2007): 18877.

(61) M.L. Broide, C.R. Berland, J. Pande, O.O. Ogun, G.B. Benedek, *PNAS* 88 (1991): 5660.

(62) G.M. Thurston, *Journal of Chemical Physics* 124 (2006): 134909.

(63) M. Muschol and F. Rosenberger. *Journal of Chemical Physics* 107 (1997): 1953.

(64) W.C.K.Poon, *J. Phys. Condens. Mat*. 14 (2002): R859.

(65) M.R. Parsek, E.P. Greenberg, *PNAS* 97 (2000): 8789.

(66) D. Liu, P.W. Thomas, J. Momb, Q.Q. Hoang, G.A. Petsko, D. Ringe, W. Fast, *Biochemistr*y 46 (2007): 11789.

(67) S.A.Lesley, I.A.Wilson, *Journal of Structural and Functional Genomics* 6 (2005): 71.

(68) S. Selimovic, F. Gobeaux, S. Fraden, Submitted to *Lab Chip* (2009).

(69) H. Boukellal, S. Selimovic, Y. Jia, C. Cristobal, S. Fraden, *Lab Chip* 9 (2009): 331.

(70) J.U. Shim, G. Cristobal, D.R. Link, T. Thorsen, Y. Jia, K. Piattelli, S. Fraden, *JACS* 129 (2007): 8825.

(71) S. Selimovic, Y. Jia, S. Fraden, *Crystal Growth & Design*, 9 (2009): 1806.

(72) C.L. Hansen, E. Skordalakes, J.M. Berger, S.R. Quake, *PNAS* .99 (2002): 16531.

(73) C.J. Gerdts, V. Tereshko, M.K. Yadav, I. Dementieva, F. Collart, A. Joachimiak, R.C. Stevens, P. Kuhn, A. Kossiakoff, R. Ismagilov, *Angew Chem Int EdEngl*. 45 (2006): 8156.

(74) O. Galkin, P.G. Vekilov, *J. Phys. Chem. B* 103 (1999): 10965.

(75) P.G. Vekilov, L.A. Monaco, B.R. Thomas, V. Stojanoff, F. Rosenberger, *Acta Crystallogr., Sect. D* 52 (1996): 785.

(76) P.G. Vekilov, O. Galkin, *Colloids and Surfaces A: Physicochem. Eng. Aspects* 215 (2003): 125.

(77) K.A. Fichthorn, W.H. Weinberg, *J. Chem. Phys.*. 95 (1991): 1090.

(78) E. Forsythe, F. Ewing, M. Pusey, *Acta Cryst*. D50 (1994): 614.

(79) J. Berthou, P. Jolles, *Biochimica et Biophysica Acta* 336 (1974): 222.

(80) P.N. Bowerman, R.G. Nolty, E.M. Scheuer, *IEEE Transactions on Reliability* 39 (1990): 158.

(81) J.H. Ahrens, U. Dieter, *ACM Transactions on Mathematical Software* 8 (1982): 163.